ACCEPTED MANUSCRIPT

Fourier series-based approximation of time-varying parameters in ordinary differential equations

To cite this article before publication: Anna Fitzpatrick et al 2024 Inverse Problems in press https://doi.org/10.1088/1361-6420/ad1fe5

Manuscript version: Accepted Manuscript

Accepted Manuscript is "the version of the article accepted for publication including all changes made as a result of the peer review process, and which may also include the addition to the article by IOP Publishing of a header, an article ID, a cover sheet and/or an 'Accepted Manuscript' watermark, but excluding any other editing, typesetting or other changes made by IOP Publishing and/or its licensors"

This Accepted Manuscript is © 2024 IOP Publishing Ltd.

During the embargo period (the 12 month period from the publication of the Version of Record of this article), the Accepted Manuscript is fully protected by copyright and cannot be reused or reposted elsewhere.

As the Version of Record of this article is going to be / has been published on a subscription basis, this Accepted Manuscript will be available for reuse under a CC BY-NC-ND 3.0 licence after the 12 month embargo period.

After the embargo period, everyone is permitted to use copy and redistribute this article for non-commercial purposes only, provided that they adhere to all the terms of the licence https://creativecommons.org/licences/by-nc-nd/3.0

Although reasonable endeavours have been taken to obtain all necessary permissions from third parties to include their copyrighted content within this article, their full citation and copyright line may not be present in this Accepted Manuscript version. Before using any content from this article, please refer to the Version of Record on IOPscience once published for full citation and copyright details, as permissions may be required. All third party content is fully copyright protected, unless specifically stated otherwise in the figure caption in the Version of Record.

View the article online for updates and enhancements.

Fourier Series-Based Approximation of Time-Varying Parameters in Ordinary Differential Equations

Anna Fitzpatrick, Molly Folino, Andrea Arnold*

Department of Mathematical Sciences, Worcester Polytechnic Institute, Worcester, MA, USA

* Corresponding author: anarnold@wpi.edu

Abstract

Many real-world systems modeled using differential equations involve unknown or uncertain parameters. Standard approaches to address parameter estimation inverse problems in this setting typically focus on estimating constants; yet some unobservable system parameters may vary with time without known evolution models. In this work, we propose a novel approximation method inspired by the Fourier series to estimate time-varying parameters in deterministic dynamical systems modeled with ordinary differential equations. Using ensemble Kalman filtering in conjunction with Fourier series-based approximation models, we detail two possible implementation schemes for sequentially updating the time-varying parameter estimates given noisy observations of the system states. We demonstrate the capabilities of the proposed approach in estimating periodic parameters, both when the period is known and unknown, as well as non-periodic time-varying parameters of different forms with several computed examples using a forced harmonic oscillator. Results emphasize the importance of the frequencies and number of approximation model terms on the time-varying parameter estimates and corresponding dynamical system predictions.

Keywords: Nonstationary inverse problems; parameter estimation; approximation models; Bayesian inference; Fourier series; ensemble Kalman filter; dynamical systems.

1 Introduction

Many real-world problems in science and engineering involve unknown model parameters of interest that may vary with time but cannot be directly observed. For example, forced harmonic oscillators used in modeling gear systems [1,2], RLC circuits [3], and cantilever motion in atomic force microscopy [4] may involve time-dependent stiffness, mass, and/or external forcing parameters. Examples in biology and medicine include time-dependent transmission parameters in modeling epidemic dynamics [5–7], external stimuli in modeling neuron dynamics [8–10], and tissue optical properties in modeling laser-tissue interactions [11,12]. The work in this paper aims to address the estimation of such time-varying parameters (TVPs)

in deterministic dynamical systems, when the parameters are not observable and there is not a known (or available) model governing their time evolution.

While TVPs may appear in different types of mechanistic models, here we focus on deterministic dynamical systems modeled using differential equations. In particular, we assume an ordinary differential equation (ODE) model of the form

$$\frac{dx}{dt} = f(t, x, \theta), \quad x(0) = x_0 \tag{1}$$

where $t \in \mathbb{R}$ denotes time, $x = x(t) \in \mathbb{R}^d$ is the vector of model states, $\theta \in \mathbb{R}^p$ is the vector of unknown model parameters, and $f : \mathbb{R} \times \mathbb{R}^d \times \mathbb{R}^p \to \mathbb{R}^d$ is a known mapping representing the state dynamics. The ODE model in (1) may involve unknown constant parameters (including the initial conditions x_0), but here we focus our attention primarily on estimating the unknown time-varying parameters of interest. Further, while such problems may generally include more than one parameter changing with time, we restrict our examples in this work to estimate a single, univariate TVP, $\theta = \theta(t) \in \mathbb{R}$, for each system. The inverse problem considered is therefore to estimate $\theta(t)$, along with the system states x(t), at some discrete times t_j given noisy, sequential observations of the system states (which may be fully or partially observed). Note that we can extend the inverse problem to include estimation of additional constant parameters, including initial conditions, as needed.

To address the inverse problem at hand, in this work we propose an approximation method inspired by the Fourier series, where we represent $\theta(t)$ as a linear combination of a finite number of sine and cosine functions and estimate the unknown coefficients of the approximation model using ensemble Kalman filtering. Fourier series-based approaches have been used in previous work for approximating smooth, periodic functions and trajectories in control systems [13,14], for linear function approximation in reinforcement learning [15], and for approximating solutions to differential equations via spectral methods [16,17]. Fourier series expansion has also been used for estimating smooth, periodic TVPs in the setting of adaptive control [18–21], where the period of the parameter is assumed to be known. We aim to approximate more general $\theta(t)$ in this work, specifically periodic parameters for which the period is not known and parameters that are time-varying but not periodic over the time interval of available system observations.

The proposed method introduces a new way of embedding Fourier series-based function approximation into the setting of parameter estimation inverse problems to estimate time-dependent physical parameters of the governing ODE system. Use of a Bayesian filtering approach such as ensemble Kalman filtering provides a flexible framework for addressing this inverse problem and allows for the unknown approximation model coefficients to be updated sequentially along with the system states as new data arrive, without relying on the full time series of data in advance. Ensemble-based methods also provide a natural measure of uncertainty in the resulting parameter estimates, generally taken as ± 2 standard deviations around the sample mean at each time. While originally developed for state estimation of partially observed systems, ensemble Kalman methods have been successfully used to solve a variety of inverse problems [22–26], including constant parameter estimation in ODEs [27]. In the setting of TVP estimation, previous studies have used Bayesian filtering approaches to estimate the constant coefficients of piecewise functional representations of periodic parameters [28, 29], constant parameters for linear TVP models [30], and in conjunction with

parameter tracking schemes to estimate more general time-varying forms [10,31–35]. Recent works have also addressed the related problems of approximating hidden physics and/or latent system dynamics through use of data-driven and machine learning techniques [36–38].

1.1 Contributions

The approach presented in this work focuses on recovering unknown and unmeasured dynamical system parameters with time-dependent behavior, updating the parameterization of the physical model through use of a sinusoidal representation of the underlying TVP. In essence, this method utilizes a dictionary of sinusoidal functions inspired by the Fourier series terms and weighted with coefficients estimated online by ensemble Kalman filtering to sequentially update the TVP approximation. The main contributions of this work include:

- A new method for estimating TVPs in dynamical systems, wherein sinusoidal functions inspired by Fourier series terms are used in a dictionary to generate an approximation model for the TVP, thereby transforming the TVP estimation into a constant coefficient estimation inverse problem;
- Two implementation options for sequentially updating the TVP approximations, both using an ensemble Kalman filtering framework to track the system states and estimate the unknown TVP approximation model coefficients; and
- Strategies for using this method to estimate periodic parameters both when the period is known and unknown, as well as extensions to estimate TVPs that are not periodic over the time interval of available data.

In a set of numerical examples considering a forced mass-spring system, we first establish the ability of the proposed Fourier series-based approximation approach to estimate a periodic forcing parameter with known period, then extend the estimation to include the period of the TVP as an additional unknown. We further demonstrate the capability of the proposed method in estimating TVPs that are not periodic (and potentially not continuous) over the time interval of observed data and show that the resulting parameter approximation models can be used to make reasonably accurate predictions of the system dynamics for different initial conditions. In the appendix, we include additional numerical results comparing the proposed approach with a standard augmented ensemble Kalman filtering algorithm and parameter tracking techniques, as well as an example considering a periodically-forced, partially observed Lorenz system with chaotic behavior.

We remark that the focus of this work does not immediately lie on application to largescale problems using small ensemble sizes or on systems with chaotic dynamics (as is common in the data assimilation literature) but rather on establishing a method to well estimate the functional form (shape and magnitude) of the underlying TVP. Even for small systems (e.g., where d=2 or 3), the number of unknown coefficients grows with the number of terms used in the TVP approximation model, thereby requiring use of an ensemble size larger than the number of system states. We discuss considerations including the choice of the number of approximation model terms needed to well represent the underlying TVP in this work.

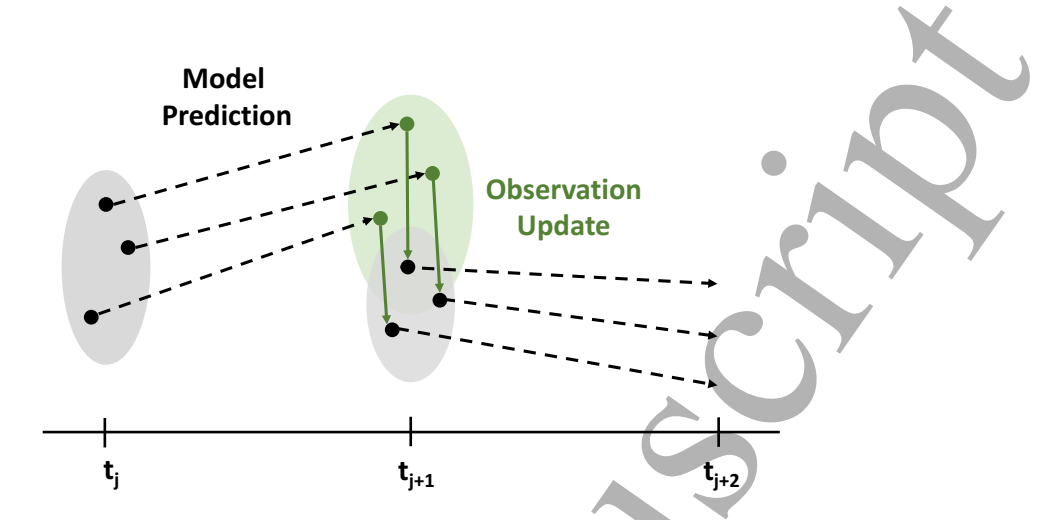


Figure 1: Illustration of the EnKF two-step updating scheme. In the model prediction step, the ensemble members (represented as black circles, with sample variance in gray) at time j are propagated forward (shown with black dashed arrows) to time j+1 by solving the model in (13). In the observation update, the ensemble predictions (green circles) are corrected (green arrows) using the observed system data at time j+1. The process continues using the corrected sample at time j+1 (black circles) until all available data are assimilated.

1.2 Paper Organization

The remainder of the paper is organized as follows: Section 2 briefly reviews ensemble Kalman filtering for constant parameter estimation. Section 3 details the proposed Fourier series-based TVP approximation models, providing two implementation approaches that can be used together with ensemble Kalman filtering to estimate the unknown model coefficients. Section 4 provides the main results of the numerical experiments (with some additional results provided in the appendix), and Section 5 gives conclusions and future work.

2 Review: Ensemble Kalman Filtering for Sequential Estimation of Constant Parameters

In this section, we briefly review the main ideas behind ensemble Kalman filtering for combined state and constant parameter estimation. While the method was originally established for tracking unobserved model states [39, 40], the augmented approach outlined below has been successfully used to estimate constant parameters in a variety of models, including systems of ODEs [27]. For a recent review of ensemble Kalman filtering, we refer interested readers to [41].

The Ensemble Kalman Filter (EnKF) is a sequential Bayesian approach that employs ensemble statistics within the framework of the classic Kalman filter to track unknown model variables given observed time series data. The incorporation of a statistical sample, which represents an underlying probability distribution of the unknowns conditioned on the available data, accommodates the use of nonlinear and possibly non-Gaussian models. The

```
Algorithm 1: EnKF for Combined State and Constant Parameter Estimation
    Input: Initial sample S_0 drawn from prior distribution \pi(x_0, \theta_0)
    Output: Posterior sample S_T and corresponding ensemble statistics
1 Initialize time index j=0
2 while j < T do
          /* Prediction Step
          for n = 1, \ldots, N do
3
                x_{j+1}^{(n)} = F(x_j^{(n)}, \theta_j^{(n)}) + v_{j+1}^{(n)}, \quad v_{j+1}^{(n)} \sim \mathcal{N}(0, \mathsf{C})   z_{j+1}^{(n)} = \left[ x_{j+1}^{(n)}; \theta_j^{(n)} \right] 
4
          /* Observation Update
          for n = 1, \ldots, N do
6
             \begin{bmatrix} y_{j+1}^{(n)} = y_{j+1} + w_{j+1}^{(n)}, & w_{j+1}^{(n)} \sim \mathcal{N}(0, \mathsf{D}) \\ z_{j+1}^{(n)} = z_{j+1}^{(n)} + \mathsf{K}_{j+1} \big( y_{j+1}^{(n)} - G(z_{j+1}^{(n)}) \big) \end{bmatrix} 
          /* Compute Posterior Ensemble Statistics
                                                                                                                                                                */
       \begin{split} \bar{z}_{j+1} &= \frac{1}{N} \sum_{n=1}^{N} z_{j+1}^{(n)} \\ \Gamma_{j+1} &= \frac{1}{N-1} \sum_{n=1}^{N} (z_{j+1}^{(n)} - \bar{z}_{j+1}) (z_{j+1}^{(n)} - \bar{z}_{j+1})^{\mathrm{T}} \\ /* \text{ Update Time Index} \end{split}
                                                                                                                                                                */
          j = j + 1
```

EnKF can estimate unobserved (or unobservable) model states along with unknown constant parameters through use of an augmented dynamical system

$$\frac{dz}{dt} = \begin{bmatrix} \frac{dx}{dt} \\ \frac{d\theta}{dt} \end{bmatrix}, \quad z(0) = \begin{bmatrix} x(0) \\ \theta(0) \end{bmatrix} \in \mathbb{R}^{d+p}$$
 (2)

where dx/dt describes the system dynamics, as given in (1), while $d\theta/dt$ represents the dynamics of the parameters [22, 27]. In particular, $d\theta/dt = 0$ when the parameters are constant (i.e., time-invariant).

Given a discrete sample of the model states and parameters at time j,

$$S_j = \left\{ (x_j^{(1)}, \theta_j^{(1)}), \dots, (x_j^{(N)}, \theta_j^{(N)}) \right\}$$
(3)

the EnKF works as a two-step updating scheme: First, each pair of states and parameters is predicted at time j + 1 using the evolution model in (2); then, the augmented vectors are corrected using the Kalman filter observation updating equation, which incorporates the observed data at time j + 1. This process is illustrated in Figure 1, and the steps of the algorithm for combined state and constant parameter estimation are outlined in Algorithm 1.

When working with ODE models, the operator F in the prediction step of Algorithm 1 (line 4) denotes the numerical solution to the differential equations model in (1) at time j+1; the parameter values are not updated during this step. In the observation update, y_{j+1} in line 7 denotes the vector of observed model states, with dimension $m \leq d$, which is perturbed

to help avoid too low a covariance in the resulting sample [40]. The updating equation in line 8 corrects the joint predicted sample for each n using the Kalman gain matrix K_{j+1} and the difference between the perturbed observation $y_{j+1}^{(n)}$ and predicted observation $G(z_{j+1}^{(n)})$, where G is the observation model. For linear observations, $G(z_{j+1}^{(n)}) = \mathsf{P} z_{j+1}^{(n)}$, where $\mathsf{P} \in \mathbb{R}^{m \times (d+p)}$ is a projection matrix whose entries corresponding to observed states are 1 and entries corresponding to unobserved states and parameters are 0. The posterior ensemble statistics computed in lines 9 and 10 give the mean and covariance, respectively, of the resulting sample at time j+1. The posterior mean for each parameter is taken as its estimate, with uncertainty commonly represented using ± 2 standard deviations around the mean. The process repeats sequentially until all available data in the time series are assimilated. In this procedure, the parameter values are artificially evolved with the aim of converging to a constant.

3 Fourier Series-Based Approximation Models for Time-Varying Parameters

While the EnKF algorithm reviewed in Section 2 is formulated for estimating constant parameters, our goal in this work is to estimate time-varying system parameters for which no evolution model is known (or available); i.e., we do not have a known form of $d\theta/dt$ for $\theta = \theta(t)$. To address this problem, we propose a novel approximation method inspired by the Fourier series, where $\theta(t)$ is represented as a linear combination of sine and cosine functions with different frequencies. We describe this approach below, detailing formulations for estimating periodic parameters when the period of $\theta(t)$ is both known and unknown, as well as for approximating more general TVPs that are not periodic over the time interval of observed data. We provide two possible implementation strategies using the EnKF for coefficient estimation.

3.1 Fourier Series and Approximation Model Formulation

Recall that the Qth order Fourier series of a univariate function h(t) is given by

$$h(t) = \frac{a_0}{2} + \sum_{q=1}^{Q} \left(a_q \cos\left(\frac{2\pi qt}{P}\right) + b_q \sin\left(\frac{2\pi qt}{P}\right) \right)$$
 (4)

where a_q and b_q are the expansion coefficients and P is the period. If h(t) is known, the coefficients a_q and b_q can be computed explicitly using the formulas

$$a_q = \frac{2}{P} \int_0^P h(t) \cos\left(\frac{2\pi qt}{P}\right) dt \tag{5}$$

and \

$$b_q = \frac{2}{P} \int_0^P h(t) \sin\left(\frac{2\pi qt}{P}\right) dt \tag{6}$$

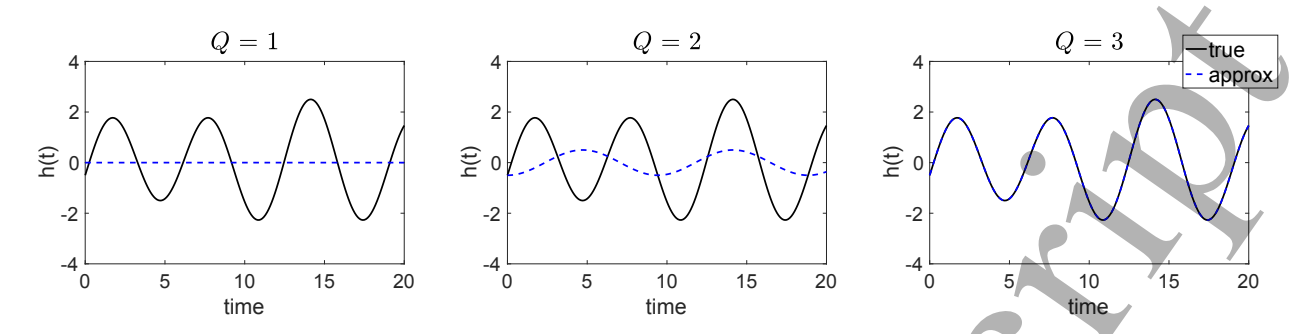


Figure 2: Fourier series approximations of the sinusoidal function $h(t) = 2\sin(t) - 0.5\cos(2t/3)$ using different values of Q, which dictates the number of terms used in the approximation. In each plot, the Fourier series approximation is shown in dashed blue, while the true function is shown in solid black. The integrals in (5) and (6) were computed numerically using adaptive quadrature via the integral function in MATLAB [42].

respectively. For example, Figure 2 shows the Fourier series approximations of the periodic function $h(t) = 2\sin(t) - 0.5\cos(2t/3)$ with known period $P = 6\pi$ for different choices of Q. However, when using Fourier series for function approximation, the function h(t) is generally unknown and the coefficients a_q and b_q must be estimated [15, 18, 20].

Inspired by use of the Fourier series for approximating unknown functions, we propose to represent the unknown, univariate time-varying parameters $\theta(t)$ in this work as linear combinations of sine and cosine pairs, such that the estimate of each $\theta(t)$ is determined by the approximation model

$$\theta_M(t) = \alpha_0 + \sum_{i=1}^{M} \left(\alpha_i \sin(\omega_i t) + \beta_i \cos(\omega_i t) \right)$$
 (7)

with coefficients α_i , β_i and fixed values of ω_i for each $i=1,\ldots,M$. Moving forward, we denote the 2M+1 coefficients by c_k , $k=0,\ldots,2M$, such that the model in (7) becomes

$$\theta_M(t) = c_0 + c_1 \sin(\omega_1 t) + c_2 \cos(\omega_1 t) + \dots + c_{2M-1} \sin(\omega_M t) + c_{2M} \cos(\omega_M t)$$
 (8)

for some fixed M. Our goal in approximating $\theta(t)$ is therefore is to estimate the 2M+1 coefficients c_k that provide the best fit between the model in (8) and the true time-varying parameter given the observed system data. This essentially transforms the inverse problem at hand into a constant parameter estimation problem, and we can utilize the EnKF algorithm described in Section 2 to estimate these coefficients. We remark that this problem is similar in spirit to dictionary learning, where writing the TVP approximation model in (8) equivalently as

$$\theta_M(t) = \begin{bmatrix} 1 & \sin(\omega_1 t) & \cos(\omega_1 t) & \cdots & \sin(\omega_M t) & \cos(\omega_M t) \end{bmatrix} c$$
 (9)

highlights the dictionary of sinusoidal functions, inspired by the Fourier series terms, and $c \in \mathbb{R}^{2M+1}$ is a vector containing the unknown coefficients c_k . The coefficient estimation thereby determines which of these functions make meaningful contributions in representing the underlying shape and magnitude of $\theta(t)$ given the available system observations.

To apply the TVP approximation model in (8), one must specify the value of M, which sets the number of terms in the approximation, and the values of ω_i , i = 1, ..., M, which

act as the angular frequencies of the sinusoidal functions. When $\theta(t)$ is periodic, we consider two different approaches in assigning the ω_i values: If we know the period of the underlying $\theta(t)$ in advance of the estimation process, we explicitly define ω_i using the formula

$$\omega_i = \frac{2\pi i}{P}, \quad i = 1, \dots, M \tag{10}$$

where P is the known period of $\theta(t)$; this form of ω_i follows from the terms in the Fourier series in (4) for approximating a periodic function with known period. If the period of $\theta(t)$ is unknown or uncertain, we set ω_i as in (10) and treat the period P as an additional unknown constant parameter to be jointly estimated along with the coefficients of the TVP approximation model. In more general cases, i.e., when $\theta(t)$ is not known to be periodic over the time interval of available data, we instead choose a fixed increment ω and define $\omega_i = \omega i$ for each $i = 1, \dots, M$, systematically incorporating sine and cosine pairs with different frequencies into the approximation. Following this approach, appropriate choice of the increment ω becomes an important factor in the estimation process.

Alternative Implementation: Derivative-Based Augmentation 3.2of System States

In the previous section, we propose an approximation model for $\theta(t)$ that we can use directly within the ODE model in (1) in place of the TVP. As an alternative means of implementation, much in the spirit of state augmentation, we can use the approximation model in (8) to prescribe a model for $d\theta/dt$ and define a coupled ODE system of the form

$$\frac{dx}{dt} = f(t, x, \theta), \quad x(0) = x_0 \tag{11}$$

$$\frac{dx}{dt} = f(t, x, \theta), \quad x(0) = x_0$$

$$\frac{d\theta}{dt} = \theta'_M(t), \quad \theta(0) = \theta_0$$
(11)

which we can write equivalently as the augmented system

$$\frac{dz}{dt} = \begin{bmatrix} \frac{dx}{dt} \\ \frac{d\theta}{dt} \end{bmatrix} = \begin{bmatrix} f(t, x, \theta) \\ \theta'_M(t) \end{bmatrix}, \quad z(0) = z_0 = \begin{bmatrix} x_0 \\ \theta_0 \end{bmatrix}$$
(13)

where $z=z(t)\in\mathbb{R}^{d+1}$. In this representation, $\theta=\theta(t)$ is treated as an unobserved state of the system in (13). The equation for $d\theta/dt$ in (13) follows from taking the derivative of the approximation model $\theta_M(t)$ in (8), which gives

$$\theta_M'(t) = c_1 \omega_1 \cos(\omega_1 t) - c_2 \omega_1 \sin(\omega_1 t) + \dots + c_{2M-1} \omega_M \cos(\omega_M t) - c_{2M} \omega_M \sin(\omega_M t)$$
 (14)

with 2M unknown coefficients, c_1, \ldots, c_{2M} . Note that the additive constant c_0 no longer explicitly appears in the system equations; instead, we estimate the initial condition θ_0 as an additional constant parameter playing a similar role.

4 Numerical Results

In this section, we detail the results of several numerical experiments demonstrating the effectiveness of the proposed methodology under different scenarios for $\theta(t)$; more specifically, we consider examples where $\theta(t)$ is a periodic TVP, in cases assuming both a known period and an unknown period, and where $\theta(t)$ is a non-periodic TVP over the time interval of available system data. Results were obtained using MATLAB (The MathWorks, Inc., Natick, MA) programming language.

As a test system in the computed examples that follow, we consider a forced harmonic oscillator, classically modeled using the second-order ODE

$$mp'' + bp' + kp = \theta(t) \tag{15}$$

where p = p(t) commonly denotes the position (or displacement) of a mass at time t, m > 0 is the constant mass, b > 0 is the damping coefficient, and k > 0 is the spring constant; see, e.g., [43,44]. Here $\theta(t)$ represents external forcing applied to the system, which we treat as our time-varying parameter of interest. Letting v(t) = p'(t) denote the velocity of the mass, we can rewrite (15) as a first-order ODE system of the form

$$\frac{dp}{dt} = v \tag{16}$$

$$\frac{dv}{dt} = \frac{1}{m} \left(-kp - bv + \theta(t) \right) \tag{17}$$

or, equivalently, as

$$\frac{dx}{dt} = \begin{bmatrix} 0 & 1\\ -\frac{k}{m} & -\frac{b}{m} \end{bmatrix} x + \begin{bmatrix} 0\\ \frac{\theta(t)}{m} \end{bmatrix}$$
 (18)

where $x(t) = [p(t); v(t)] \in \mathbb{R}^2$ is the vector of model states at time t. Assuming that the constants m, k, and b are known, our goal is to estimate $\theta(t)$ using the Fourier series-based approximation methods described in Section 3. (We note that additional results, including an example using a periodically-forced Lorenz system with chaotic behavior, are provided in the appendix.)

To test the effectiveness of the proposed estimation techniques, we generate data from the mass-spring system in (18) using the initial condition x(0) = [2; 0], fixed constants m = 10, k = 5, and b = 3, and different forms of the time-varying forcing parameter $\theta(t)$, as detailed for each experiment below. We initialize the EnKF with a sample size of N = 100 and draw the prior ensemble of state values from a multivariate Gaussian distribution with mean $[1;1] \in \mathbb{R}^2$ and covariance matrix $(0.5)^2 I_2$, where I_2 denotes the 2×2 identity matrix. We draw the prior ensemble of values for each of the unknown coefficients c_k uniformly over the interval [-2,10]. Further, we use MATLAB's ode15s to solve the ODE system in (18) at each time step of the filter and prescribe $C = (0.02)^2 I_2$ as the model innovation covariance matrix and $D = (0.08)^2 I_2$ as the observation covariance matrix, assuming observations of both position and velocity.

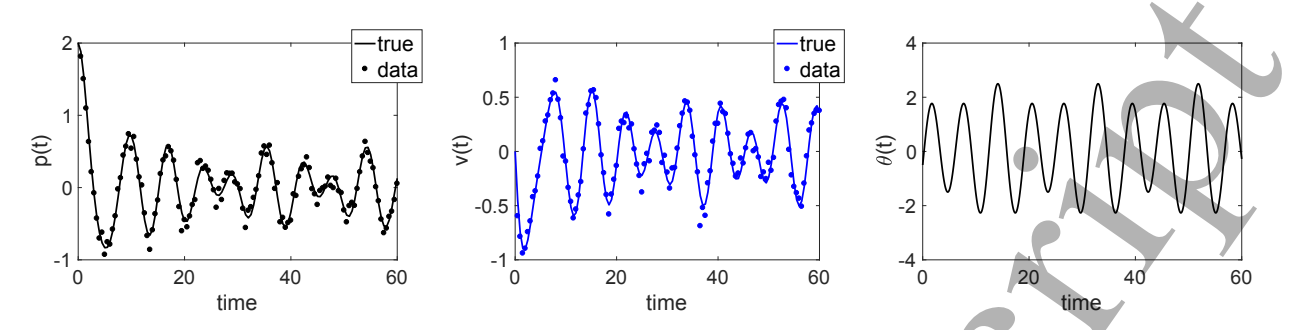


Figure 3: Position and velocity data generated from the mass-spring system in (18) with sinusoidal forcing parameter $\theta(t) = 2\sin(t) - 0.5\cos(2t/3)$.

4.1 Example: Periodic Time-Varying Parameter

In this example, we consider a sinusoidal forcing parameter of the form $\theta(t) = 2\sin(t) - 0.5\cos(2t/3)$ with period $P = 6\pi$ as the underlying truth. Utilizing MATLAB's ode45 to solve the ODE system in (18), we record observations every 0.5 time units over the interval [0,60], spanning just over three periods of $\theta(t)$, and corrupt the observations using Gaussian noise with zero mean and standard deviation taken to be 20% of the standard deviation of the true system states. Figure 3 shows the simulated data. In the experiments that follow, we consider two cases for the estimation procedure: (i) when the period of $\theta(t)$ is known, and (ii) when the period of $\theta(t)$ is unknown. Results focus on use of the TVP approximation model approach described in Section 3.1. Appendix A.1 shows an example of the corresponding numerical results when using the derivative-based augmentation approach described in Section 3.2 for the known period case.

4.1.1 Estimation with Known Period

Assuming a known period of $P=6\pi$ for $\theta(t)$, we apply the formula in (10) to set $\omega_i=i/3$, $i=1,\ldots,M$, and employ the TVP approximation model in (8) with increasing values of M, ranging from M=1 (which involves three coefficients) through M=5 (11 coefficients). In each case, the EnKF tracks the model states and estimates the unknown coefficients comprising the Fourier series-based model approximation of $\theta(t)$. As an example, Figure 4 shows the resulting EnKF time series estimates of position, velocity, and the seven TVP model coefficients when M=3. We then use the posterior sample mean of each coefficient, \bar{c}_k , $k=0,\ldots,2M$, to construct an approximation of $\theta(t)$, such that

$$\bar{\theta}_M(t) = \bar{c}_0 + \bar{c}_1 \sin(\omega_1 t) + \bar{c}_2 \cos(\omega_1 t) + \dots + \bar{c}_{2M-1} \sin(\omega_M t) + \bar{c}_{2M} \cos(\omega_M t)$$
(19)

for each M. Table 1 lists the posterior sample mean of each coefficient for each M value, and Figure 5 shows the resulting $\bar{\theta}_M(t)$ approximations in each case compared with the true $\theta(t)$. To further compare the approximations with the true $\theta(t)$, we use a scaled version of the root mean square error (RMSE), where

Scaled RMSE =
$$\frac{\text{RMSE}}{\sigma_{\theta}}$$
, RMSE = $\sqrt{\frac{1}{T} \sum_{j=1}^{T} (\theta(t_j) - \bar{\theta}_M(t_j))^2}$ (20)

and σ_{θ} is the standard deviation of $\theta(t)$. Note that the plots in Figure 5 and corresponding scaled RMSE values in Table 1 were computed at t_j values taken every 0.1 time units over [0,60], a finer time discretization than used during the filtering process.

As illustrated in Figure 4, the filter well tracks the model states for both p(t) and v(t), and the coefficient estimates converge to constant values after assimilating approximately one period of data (here, one period occurs at time $6\pi \approx 18.85$), with the ± 2 standard deviation curves representing uncertainty around the mean estimate shrinking significantly. In comparing the results for different values of M, we note that the lowest RMSE occurs when M=3 and is similar when M=4, with a small increase in error when M=5; however, all three of these M values result in reasonably close model approximations to the true $\theta(t)$, as shown in Figure 5. Further, the EnKF posterior sample means for the TVP approximation model coefficients when M=3, 4, and 5 are quite similar to the Fourier series coefficients obtained when using the formulas in (5) and (6) to approximate the function $h(t)=2\sin(t)-0.5\cos(2t/3)$ when Q=3, 4, and 5, assuming that both h(t) and $P=6\pi$ are known (i.e., $c_4=-0.5$, $c_5=2$, and $c_k=0$ for all other coefficients).

Figure 6 shows the mass-spring system model predictions using $\bar{\theta}_M(t)$ as the forcing parameter in (18) for each M with the initial condition x(0) = [1; -1], a different initial condition than used in generating the simulated data, along with the corresponding scaled RMSE values for each model state. As might be expected given the TVP approximation results, the model predictions when using M = 1 and 2 are less accurate than when using M = 3, 4, and 5, which all provide similarly accurate predictions of both position and velocity. While not shown, similar results hold for other initial conditions in this range. For predictions using initial conditions larger in magnitude with this system, e.g., x(0) = [100; -100], a similar pattern holds where the approximation models with M = 3, 4, and 5 provide the best results (i.e., lowest RMSE values), but the overall error is lower for predictions using any of the M values considered.

4.1.2 Estimation with Unknown Period

Given the same simulated data, we now assume that the period P of $\theta(t)$ is also unknown and estimate P along with the unknown approximation model coefficients for different choices of M. We draw an initial sample of P values from a uniform distribution over [15, 20], supposing that we have some reasonable prior information on a range of likely values (the true period being $6\pi \approx 18.8496$ in this case). As an example for comparison, Figure 7 shows the resulting EnKF time series estimates of the seven TVP model coefficients and period P when M=3. Table 2 lists the posterior sample mean of the estimated coefficients and P values for each M, and Figure 8 shows the resulting $\bar{\theta}_M(t)$ approximations and time series estimates of P compared with the true $\theta(t)$ and P, respectively, when M=1, 3, and 5.

Similar to the results obtained using M=3 with a known period (shown in Figure 4), we see in Figure 7 that most of the coefficient estimates converge after assimilating about one period of data; the uncertainty encoded in the ± 2 standard deviations around the mean is a bit wider but continues to decrease as more data are sequentially incorporated. The estimate of P takes more time to converge but, after assimilating about two periods of data, converges closely to the true underlying period (with a relative error of approximately 8.6124×10^{-4}). While not shown, the resulting time series estimates for both position and velocity are similar

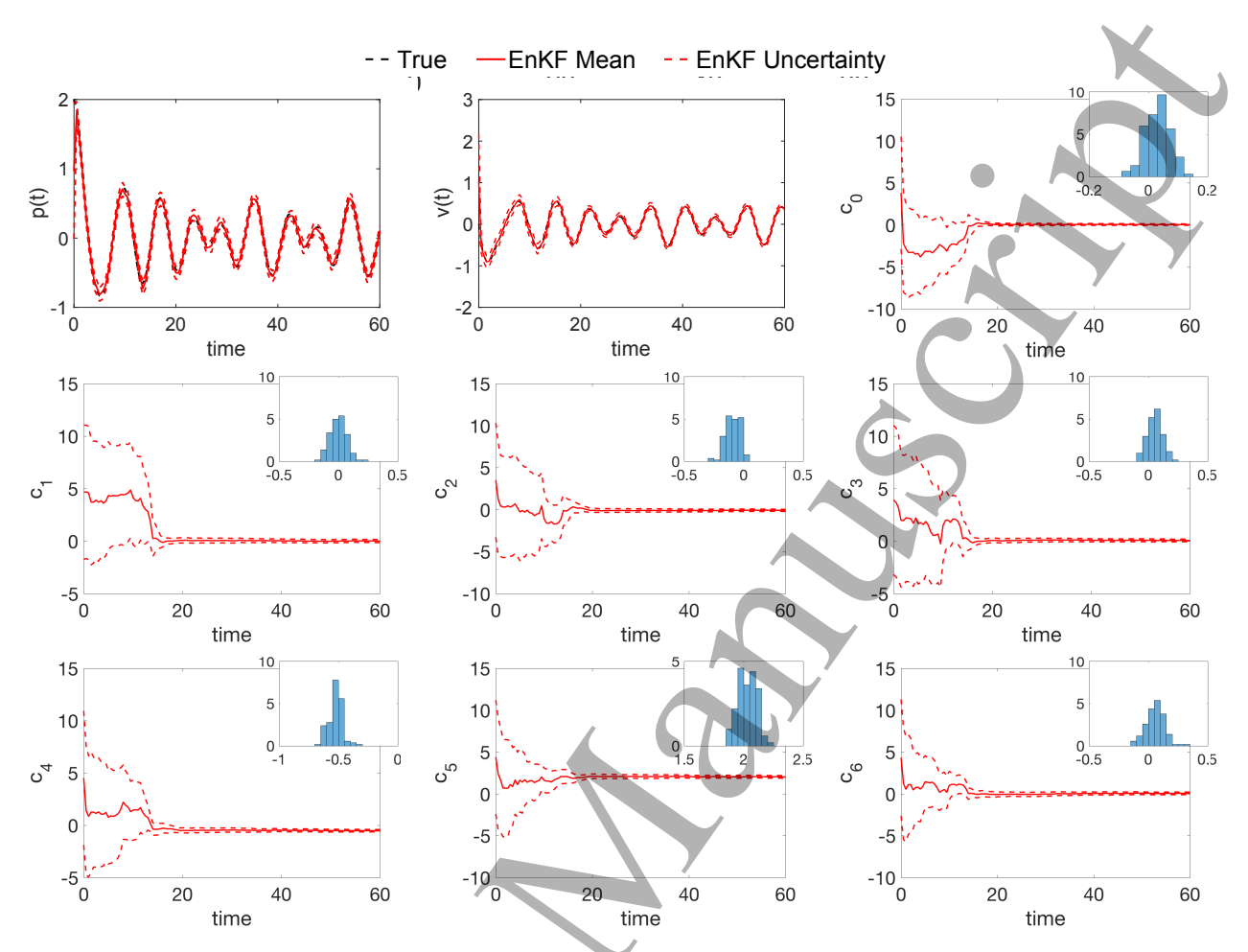


Figure 4: EnKF time series estimates of position, velocity, and the seven unknown coefficients in the TVP approximation model (8) of the sinusoidal forcing parameter $\theta(t) = 2\sin(t) - 0.5\cos(2t/3)$ in (18) when M = 3, using the data in Figure 3 and assuming a known period for $\theta(t)$. On each plot, the solid red line denotes the EnKF sample mean and the dashed red lines show ± 2 standard deviations around the mean. The plot for each coefficient, c_0, \ldots, c_6 , also shows the resulting histogram of the posterior sample at time t = 60.

to those obtained in the known period case.

The results in Table 2 and plots in Figure 8 emphasize that, again for this case, M=3 gives the best overall approximation to $\theta(t)$ (with smallest scaled RMSE) as well as the best estimate of P, with reasonably small uncertainty in this estimate by the end of the filtering process. When M=1 and M=2, the period estimates somewhat diverge from the truth and result in under-approximations. The results when M=4, while not shown graphically, are similar to M=3 but with more uncertainty in the posterior estimate of P and an increase in the scaled RMSE of the TVP approximation. When M=5, the increasing uncertainty in the posterior estimate of P becomes more clear (as seen in Figure 8), along with increased error in the TVP approximation. Following from these results, the corresponding mass-spring model predictions using different initial conditions with these TVP approximation models for $\theta(t)$ are most accurate when M=3. However, if directly using the models when

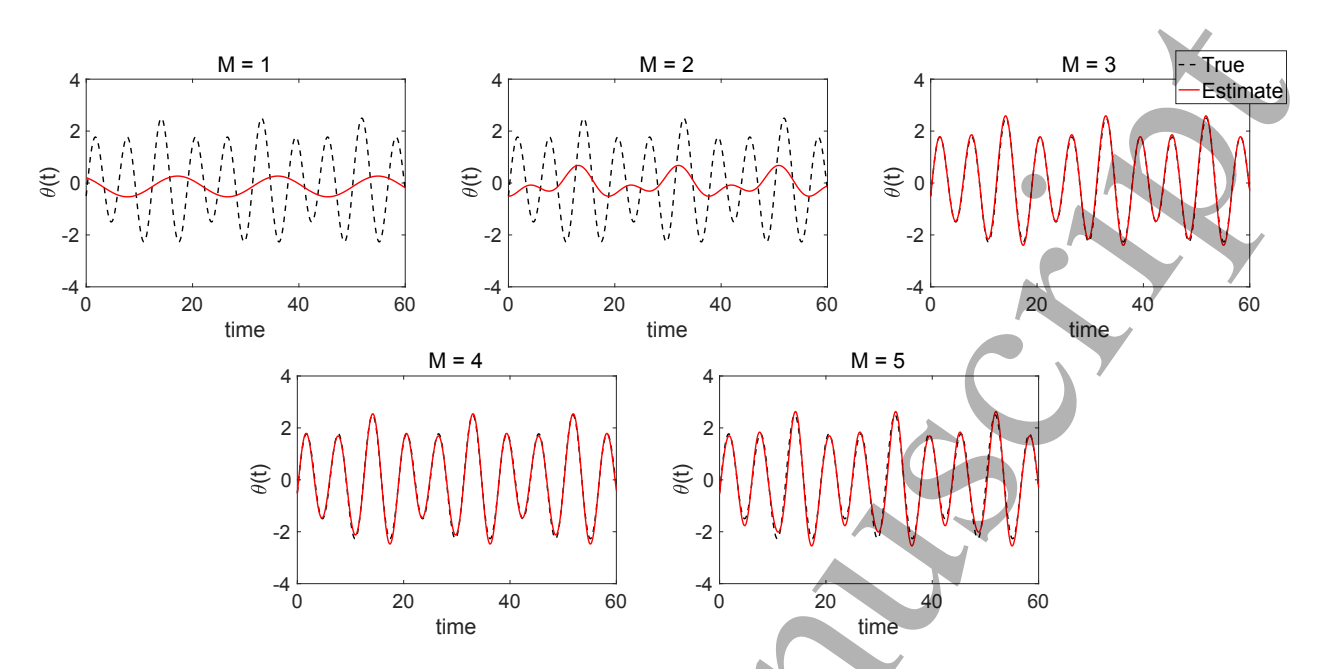


Figure 5: Resulting Fourier series-based approximations of the sinusoidal forcing parameter $\theta(t) = 2\sin(t) - 0.5\cos(2t/3)$ in (18) for different values of M, using the data in Figure 3 and assuming a known period for $\theta(t)$. On each plot, the solid red line denotes the TVP approximation $\bar{\theta}_M(t)$ computed using the posterior mean coefficient values in Table 1 and the dashed black line shows the true underlying $\theta(t)$.

M=4 or M=5 in this case, the increased uncertainty in the period and corresponding increased error in the TVP approximations lead to increased error in the model predictions. This can be addressed by using the posterior mean estimate of P, fixing the period to this known value, and re-running the filtering process (now assuming a known period) to obtain improved TVP approximation model coefficient estimates.

4.2 Example: Non-Periodic Time-Varying Parameters

In the previous simulations, we demonstrate the effectiveness of the proposed estimation method when approximating a periodic TVP, addressing situations when we know (and fix) and when we don't know (and estimate) the underlying period. Here we extend this approach to approximate more general TVP, in particular, considering cases when $\theta(t)$ is not periodic over the time interval of available data. As discussed in Section 3.1, this prevents use of a direct formula for setting the ω_i values in our sinusoidal approximation model terms. Instead, here we choose a fixed increment ω and let $\omega_i = \omega i$, i = 1, ..., M, in order to systematically include sine and cosine pairs with different frequencies in the approximation.

Using the same procedure as before, we simulate data from (18) over the time interval [0,60] with three different non-periodic forcing parameters:

(i) a linear polynomial, where
$$\theta(t) = -0.07t + 2; \tag{21}$$

Table 1: EnKF posterior sample means of the TVP model coefficients for different values of M when approximating the sinusoidal forcing parameter $\theta(t) = 2\sin(t) - 0.5\cos(2t/3)$ in (18), using the data in Figure 3 and assuming a known period for $\theta(t)$. Numbers are rounded to four decimal places. Note that the Fourier series coefficients obtained using the formulas in (5) and (6) to approximate the known function for orders 3 and above correspond to $c_4 = -0.5$, $c_5 = 2$, and $c_k = 0$ for all other coefficients.

Coefficient	M = 1	M = 2	M = 3	M = 4	M = 5
c_0	-0.1328	-0.0306	0.0303	-0.0083	-0.0552
c_1	-0.2106	-0.3373	-0.0013	-0.0000	0.0255
c_2	0.3387	-0.2012	-0.0927	-0.0624	-0.0784
c_3	_	0.1689	0.0545	0.0195	-0.0035
c_4	_	-0.2770	-0.5236	-0.5032	-0.4689
c_5	_	_	2.0299	2.0047	2.0538
c_6	_	_	0.0594	-0.0032	-0.0533
c_7	_	_	-	0.1099	0.1303
c_8	_		-7	0.0431	0.0053
c_9	_	1-		_	-0.1584
c_{10}	_	+	_	_	0.1012
Scaled RMSE	1.0211	1.0087	0.0645	0.0657	0.1282

(ii) a cubic polynomial, where

$$\theta(t) = 0.0001(t - 25)^3 - 0.001t^2 + 3; \tag{22}$$

and

(iii) a step function, where

$$\theta(t) = \begin{cases} -2 & t \le 30\\ 2 & t > 30 \end{cases}$$
 (23)

Figure 9 shows the simulated data in each case.

In building the TVP approximation models as in (8), we set an increment of $\omega = 0.01$ and define $\omega_i = 0.01i$ for each $i = 1, \ldots, M$. Since each of the underlying $\theta(t)$ have different levels of complexity, we test a variety of M values in each case. Figure 10 shows the best resulting approximations (i.e., those with the smallest corresponding scaled RMSEs) for each non-periodic forcing parameter. For the linear forcing parameter, the best fit occurs when M = 1 (with scaled RMSE ≈ 0.0239), needing only three terms in the TVP approximation model to obtain an accurate approximation. Here, increasing M to somewhat larger values (e.g., M = 4 or 5) increases the approximation error and number of unknowns but still permits reasonable approximations with convergent coefficients.

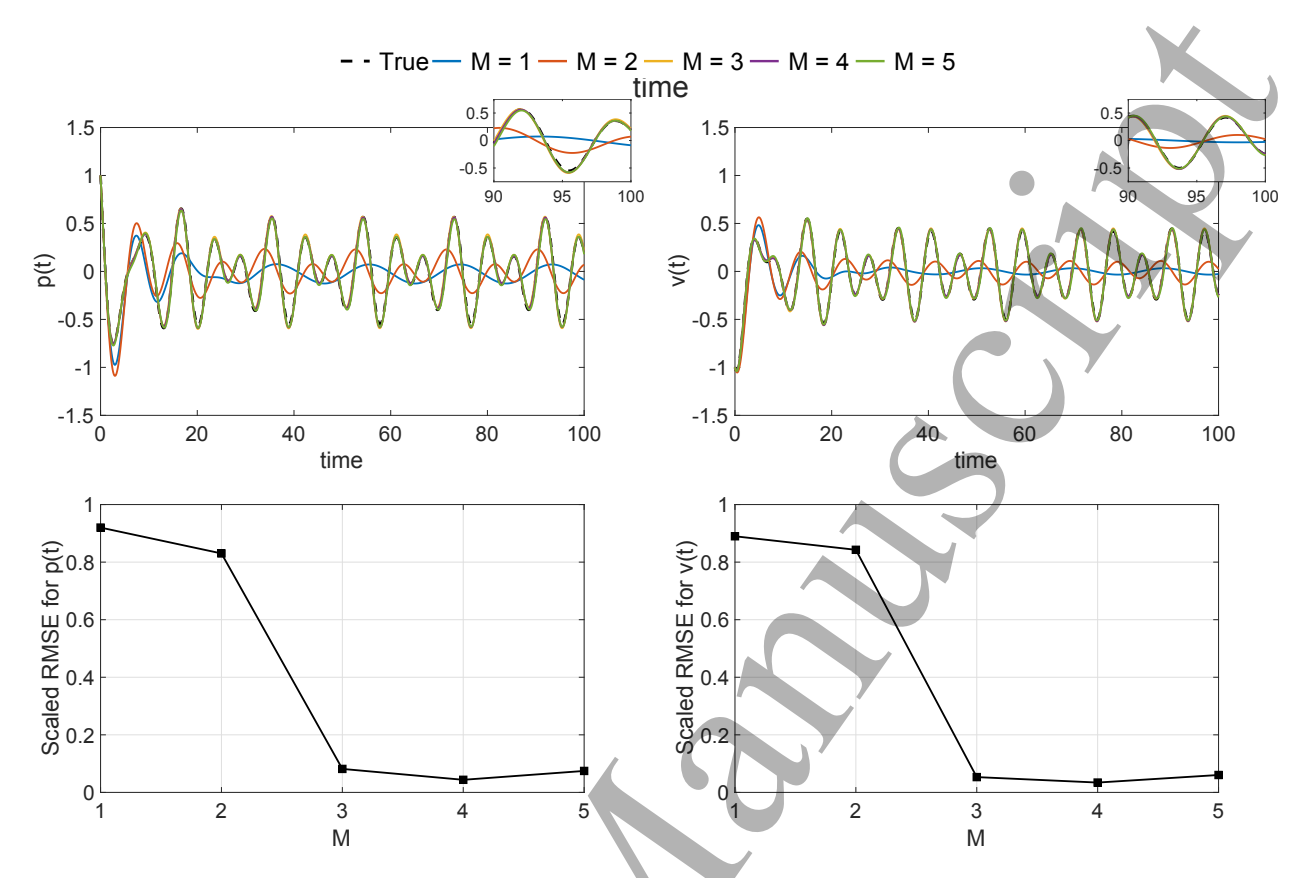


Figure 6: Top row: Predictions of position (left) and velocity (right) using initial condition p(0) = 1, v(0) = -1 and the TVP approximations for $\theta(t)$ computed with the estimated coefficients in Table 1 for different M. Bottom row: Scaled RMSE comparing the predictions of position (left) and velocity (right) with the true solutions for each M.

More terms are needed when approximating the cubic forcing parameter, and it is important to note that, for this example, using too small an M value results in coefficient estimates that do not converge over the time interval of available data. More specifically, the coefficients do not converge when M=1, 2 or 3, but convergence improves beginning with M=4. The best fit for the cubic forcing parameter occurs when M=6 (with scaled RMSE ≈ 0.1596), but with a similarly good fit when M=5 (scaled RMSE ≈ 0.1614) requiring the estimation of two less coefficients.

Estimating the step forcing parameter presents the most difficult challenge of the three, given the jump discontinuity in the function halfway through the time interval of available data. For this example, the TVP approximation model coefficients do not converge for smaller M values, but a significant increase in M leads to reasonable fits with convergent coefficients. The TVP approximations yield similar scaled RMSE values for M between 15 and 22, with the lowest occurring when M=21 (scaled RMSE ≈ 0.2737). While not capturing the exact shape, the TVP approximations in this case are able to capture the jump point between constant parameter values in the underlying step function. The mass-spring model predictions for different initial conditions follow as expected using the best TVP approximation results over the time interval [0,60], but it becomes more difficult to accurately predict the behavior of the system after this time frame for non-periodic TVPs, since the

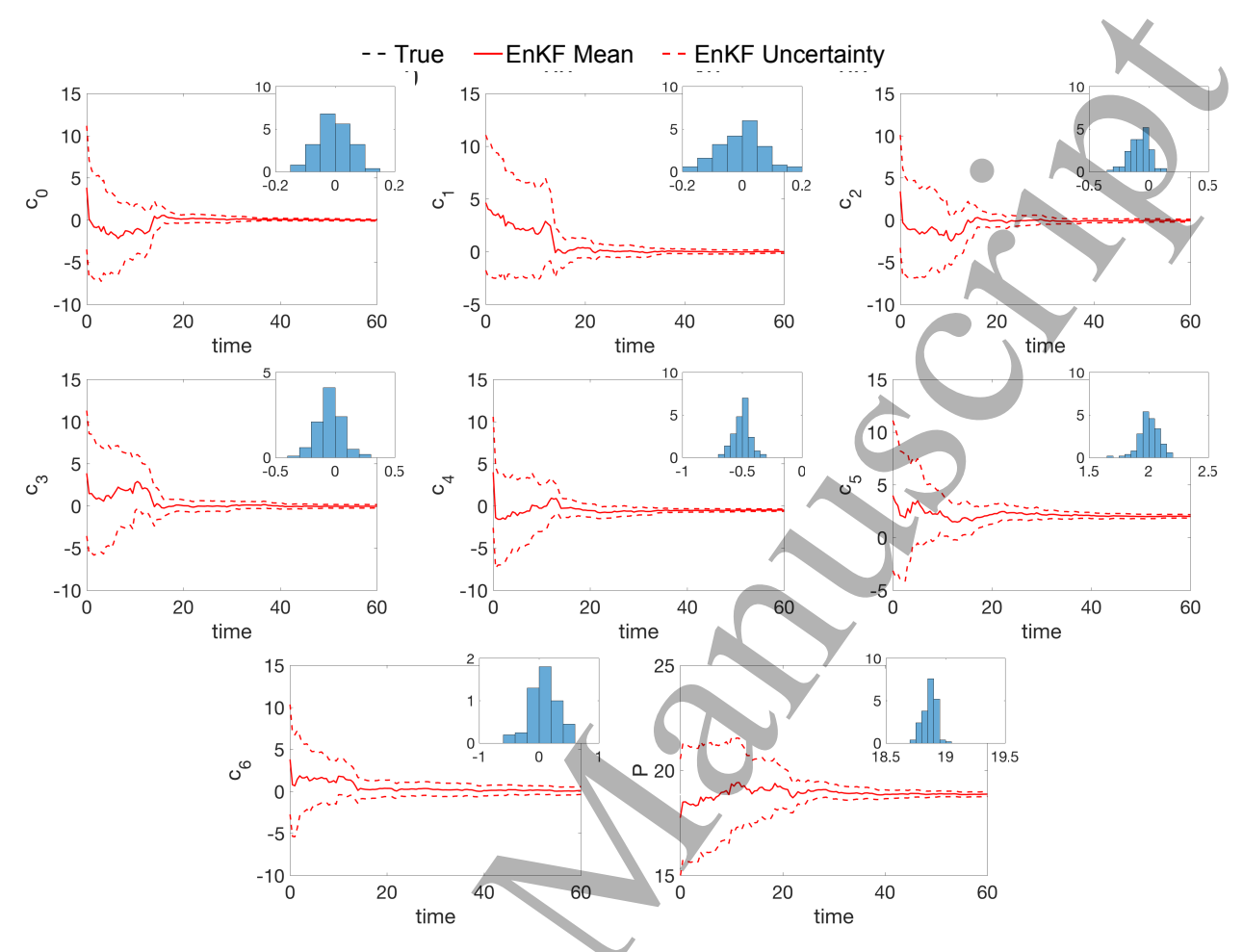


Figure 7: EnKF time series estimates of the seven unknown coefficients and period P in the TVP approximation model (8) of the sinusoidal forcing parameter $\theta(t) = 2\sin(t) - 0.5\cos(2t/3)$ in (18) when M = 3, using the data in Figure 3 and treating the period of $\theta(t)$ as an additional unknown. On each plot, the solid red line denotes the EnKF sample mean and the dashed red lines show ± 2 standard deviations around the mean. Each plot also shows the resulting histogram of the posterior sample at time t = 60.

parameters themselves will continue to dynamically change over time without updating their approximation models.

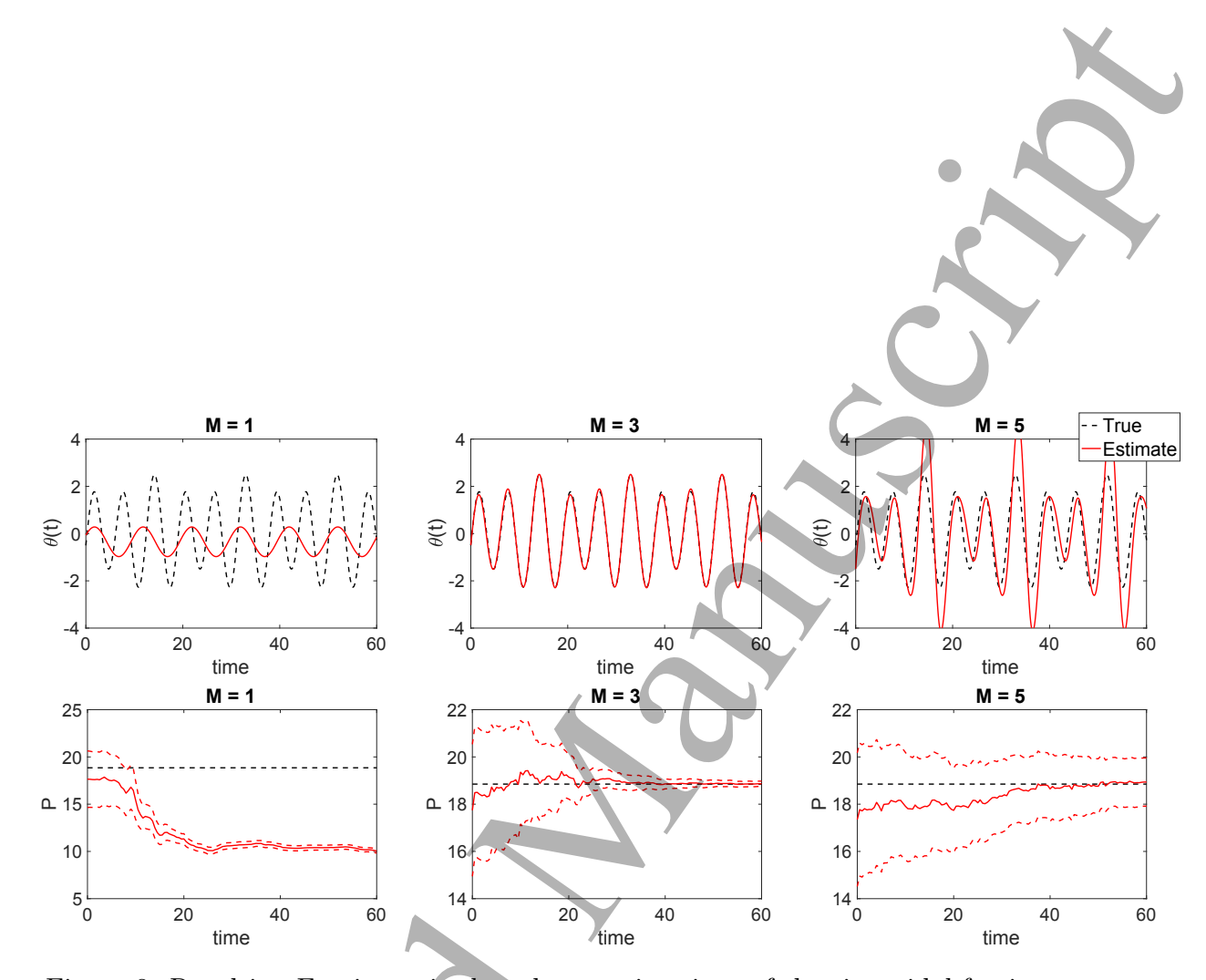


Figure 8: Resulting Fourier series-based approximations of the sinusoidal forcing parameter $\theta(t) = 2\sin(t) - 0.5\cos(2t/3)$ in (18) and corresponding time series estimates of the period P for different values of M, using the data in Figure 3 and treating the period of $\theta(t)$ as an additional unknown. Top row: On each plot, the solid red line denotes the TVP approximation $\bar{\theta}_M(t)$ computed using the posterior mean coefficient values in Table 2 and the dashed black line shows the true underlying $\theta(t)$. Bottom row: On each plot, the solid red line denotes the EnKF sample mean, the dashed red lines show ± 2 standard deviations around the mean, and the dashed black line shows the true underlying P.

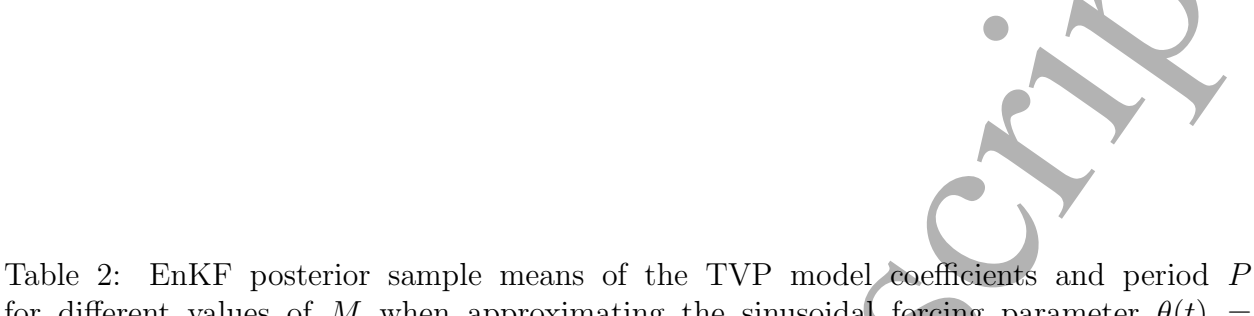


Table 2: EnKF posterior sample means of the TVP model coefficients and period P for different values of M when approximating the sinusoidal forcing parameter $\theta(t) = 2\sin(t) - 0.5\cos(2t/3)$ in (18), using the data in Figure 3 and treating the period of $\theta(t)$ as an additional unknown. Numbers are rounded to four decimal places. Note that the Fourier series coefficients obtained using the formulas in (5) and (6) to approximate the known function for orders 3 and above correspond to $c_4 = -0.5$, $c_5 = 2$, and $c_k = 0$ for all other coefficients.

Coefficient	M = 1	M=2	M = 3	M=4	M = 5
c_0	-0.3468	0.1705	-0.0053	0.0962	0.0014
c_1	0.5621	-0.0454	-0.0043	-0.0709	-0.1448
c_2	0.2776	0.0085	-0.0760	0.0274	-0.1032
c_3		1.7142	-0.0479	-0.0343	0.0747
c_4	_	-0.0627	-0.5039	-0.5476	-1.3471
c_5	_	<u>/</u>	2.0026	1.9663	2.4455
c_6		_	0.0926	-0.4897	-0.8694
c_7		_	_	0.0487	0.3266
c_8	7	_	_	-0.2534	0.4760
<i>C</i> 9		_	_	_	-0.0178
c_{10}	_	_	_	_	0.3467
P	10.0386	12.5959	18.8658	18.8024	18.9363
Scaled RMSE	1.0373	0.3170	0.0554	0.2288	0.8050

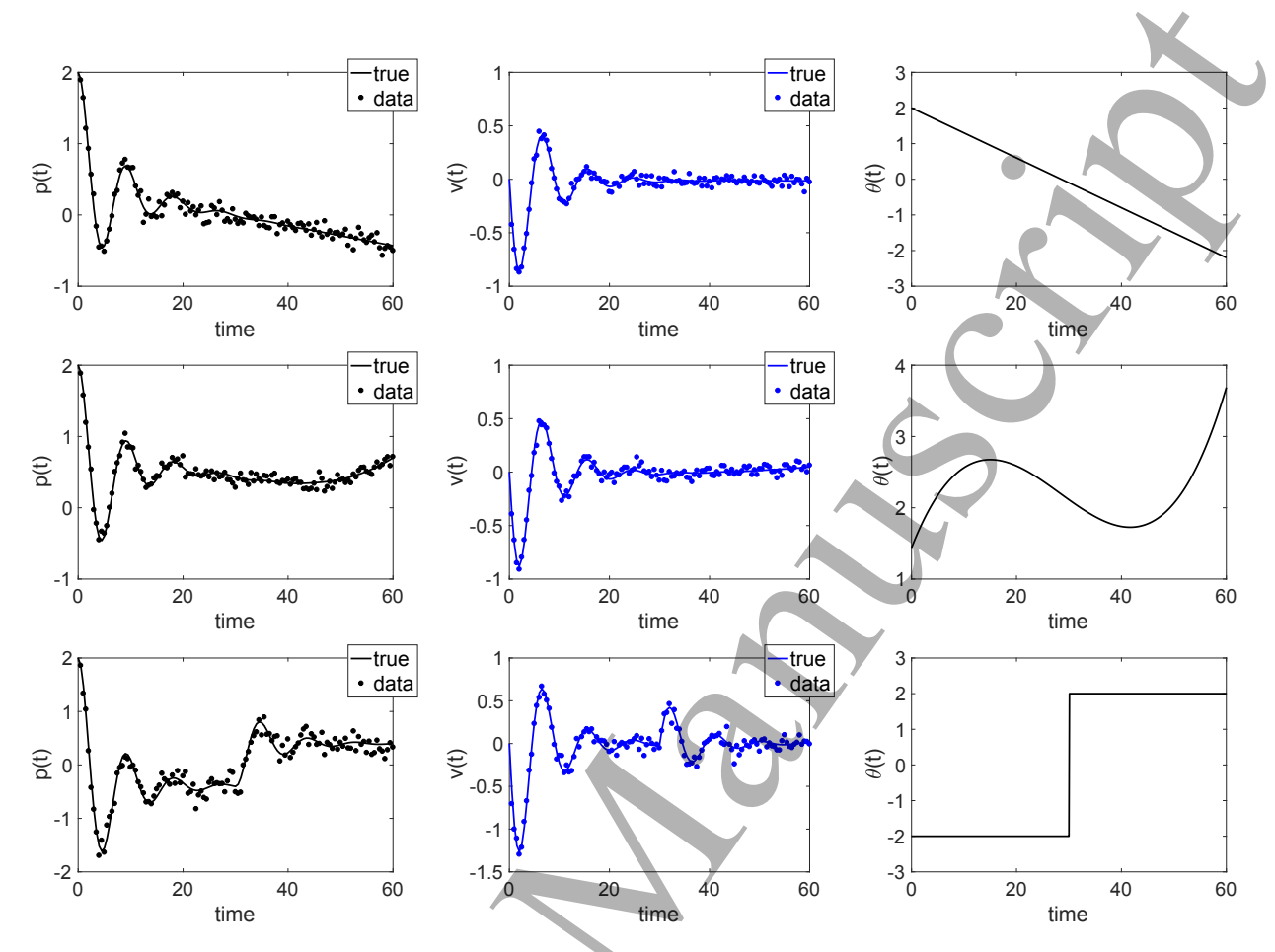


Figure 9: Position and velocity data generated from the mass-spring system in (18) with the linear forcing parameter in (21) (top row); cubic forcing parameter in (22) (middle row); and step forcing parameter in (23) (bottom row).

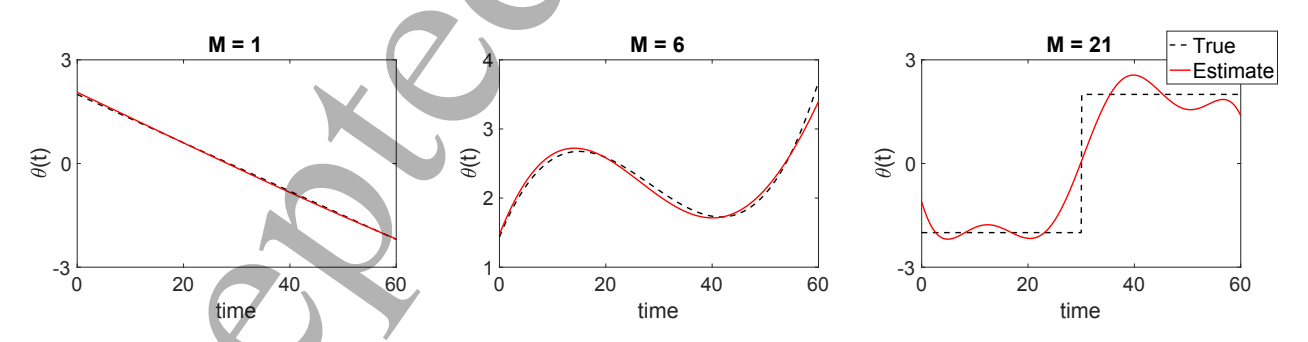


Figure 10: Resulting Fourier series-based approximations of three non-periodic forcing parameters $\theta(t)$ in (18) for the values of M yielding the smallest scaled RMSE, using the data in Figure 9 and setting $\omega_i = 0.01i$ for i = 1, ..., M in the TVP approximation models. From left to right: the linear polynomial in (21); the cubic polynomial in (22); and the step function in (23). On each plot, the solid red line denotes the TVP approximation $\bar{\theta}_M(t)$ computed using the posterior mean coefficient values and the dashed black line shows the true underlying $\theta(t)$.

5 Conclusions and Future Work

In this work, we present a novel Fourier series-based approximation method for estimating time-varying parameters in deterministic dynamical systems, where we represent $\theta(t)$ as a linear combination of sine and cosine functions and estimate the unknown approximation model coefficients using ensemble Kalman filtering. This approach allows us to construct accurate TVP approximations $\bar{\theta}_M(t)$, dependent on the integer parameter M (which dictates the number of approximation model terms) and posterior EnKF mean estimates for the model coefficients. With several numerical examples using a forced mass-spring system (see Appendix A.3 for an additional example using a periodically-forced Lorenz system with chaotic behavior), we illustrate the effectiveness of this approach in approximating TVPs of different forms, including cases when $\theta(t)$ is periodic with a known period, periodic with an unknown period (which is jointly estimated), and non-periodic over the time interval of observed data. Compared to a standard augmented EnKF or parameter tracking approach (see Appendix A.2), the proposed Fourier series-based approximation techniques show improved performance in capturing the shape and magnitude of the underlying TVP, also providing an approximation model for $\theta(t)$ (or $d\theta/dt$) that can be used in making model predictions with the ODE system.

One important aspect to consider in successfully applying this method is how to best select M in advance of running the estimation procedure. Our goal in practice is to choose the smallest integer M that will result in a reasonable TVP approximation and corresponding ODE system predictions, in order to keep the number of unknowns to a minimum as well as to reduce approximation errors from including additional terms that may not be needed. Another important consideration is how to appropriately set the angular frequencies ω_i , $i = 1, \ldots, M$, of the sinusoidal terms in the TVP approximation models. When $\theta(t)$ is periodic, we are able to set ω_i directly using the formula in (10) and either fix or estimate P, depending on what information is available. However, when estimating TVPs that are not periodic (or not known to be periodic), we select a fixed increment ω and set $\omega_i = \omega i$; the choice of this increment is vital in the resulting TVP approximation and also can affect which M is most appropriate for the problem. Future work will include incorporating model selection techniques [45, 46] and potential pre-processing steps to select M and ω systematically for a given problem.

Further, in the examples estimating periodic parameters with sinusoidal form, it is clear from the resulting TVP approximation model coefficient estimates (as well as in the Fourier series coefficients of the true parameter functions) that only a few terms in the approximation model have significant impact in well representing the underlying parameter dynamics, while a majority of the terms make small contributions that can instead introduce approximation errors. To promote a sparse representation emphasizing the most significant terms in the approximation model, in future work we aim to modify the proposed approach to incorporate sparsity preservation techniques; see, e.g., [47,48]. We anticipate that employing sparse dictionary learning will contribute to the robustness of the approach and potentially reduce some of the aforementioned concerns about the choice of M.

While application of EnKF-type methods for data assimilation in practice tend to favor use of small ensemble sizes for large-scale problems (with a large number of system states), here the number of unknown coefficients grows with M and quickly surpasses the number

of system states. Since our main goal in employing the method in this work is to well approximate the underlying $\theta(t)$, we present results using a relatively large (compared to the number of system states) ensemble size, i.e., N=100 for the numerical examples discussed. We remark that it is possible to obtain similar results using smaller ensembles, but we must be careful not to choose too small an ensemble size (i.e., less than number of unknowns) to avoid potential issues with filter divergence and degraded performance of the filter in approximating $\theta(t)$. Future work will explore application of these techniques to large-scale inverse problems, including problems with multiple TVPs to estimate (thereby increasing the number of unknown approximation model coefficients), and possible avenues for reducing the ensembles sizes in the approximation.

We note that the proposed approach is not limited to the use of EnKF in estimating the unknown coefficients and could also be implemented using different nonlinear filtering methods (e.g., particle filters [49]) with sequentially-arriving data or non-sequential Bayesian approaches (e.g., MCMC methods [50]) if the full time series of data is available at once. However, our results show that we are able to reasonably approximate the unknown TVPs of interest using the EnKF with a relatively small sample size compared to those generally needed for particle filtering or MCMC-based approaches. While the examples in this work each focus on estimating a single, univariate TVP for the system considered, future work will examine the feasibility of this approach in simultaneously estimating multiple TVPs for a given system (increasing the number of unknowns and complexity of the problem, as the different TVPs for the same system might have different periods, different known or unknown period information, and would likely require different M values for each approximation model), as well as introducing model-data mismatch as we move toward real-data application.

Acknowledgements

This work was supported by the National Science Foundation under grant number NSF/DMS-1819203 (A. Arnold).

ORCID iDs

Andrea Arnold: https://orcid.org/0000-0003-3003-882X

Appendix A Additional Numerical Results

A.1 Example Using Derivative-Based Augmentation

In this section, we apply the derivative-based augmentation approach described in Section 3.2 to estimate the sinusoidal forcing parameter $\theta(t) = 2\sin(t) - 0.5\cos(2t/3)$ in (18) using the same data as in Figure 3 and assuming a known period for $\theta(t)$. Compared to the approach used in Section 4.1.1, the difference with this implementation is that we now treat $\theta(t)$ as

unobserved system state, where

$$\frac{d\theta}{dt} = \theta_M'(t), \quad \theta(0) = \theta_0 \tag{A.1}$$

with $\theta'_M(t)$ defined as in (14), and we track it along with p(t) and v(t), estimating the 2M coefficients c_1, \ldots, c_{2M} plus the TVP initial value θ_0 for a total of 2M+1 unknown constant parameters. Figure A.1 shows the resulting EnKF time series estimates of position, velocity, and $\theta(t)$, along with the six unknown coefficients in (14) and the initial condition θ_0 , when M=3. Table A.1 lists the posterior sample mean of each coefficient and θ_0 for each M value, and Figure A.2 shows the corresponding EnKF time series estimates of $\theta(t)$ in each case compared with the true $\theta(t)$.

The results in Figure A.1 highlight the differences between this derivative-based augmented systems implementation and the direct approximation model (with corresponding results shown in Figure 4), where here $\theta(t)$ is treated as an unobserved system state and tracked along with position and velocity. The six coefficients converge after assimilating about one period of data, which is also reflected in the tracking of $\theta(t)$, while the estimate of θ_0 continues to improve over the remaining time interval of observations. As the plots in Figure A.2 illustrate, the filter is not able to well track $\theta(t)$ when M=1 and 2, noticeably under-estimating the dynamics with a damping effect beginning close to the one period mark (i.e., around time t=19). The estimation significantly improves when M=3, where the EnKF mean estimate very well captures the behavior of the true underlying parameter after assimilating one period of data, with fairly tight uncertainty bounds around the mean estimate. Similar behavior occurs when M=4 and 5, although there is more initial error in the approximation over the first period and slightly wider uncertainty bounds after the coefficients converge. The results in Table A.1 paint a similar picture for the posterior mean estimates of θ_0 , where the estimate when M = 3 yields the smallest relative error (≈ 0.1440) when compared to the true initial value $\theta_0 = -0.5$.

A.2 Comparison of Fourier Series-Based Approach with Standard Augmented EnKF and Parameter Tracking

In this section, we demonstrate the performance when applying the standard augmented EnKF algorithm described in Section 2 to estimate the sinusoidal forcing parameter $\theta(t) = 2\sin(t) - 0.5\cos(2t/3)$ in (18) using the same data as in Figure 3. Since the standard augmented EnKF is meant for estimating constant parameters, we anticipate that applying this algorithm to estimate the time-varying forcing parameter will not capture its dynamic behavior. As expected, Figure A.3 shows that the standard augmented EnKF indeed fails to capture the dynamics of $\theta(t)$ and instead converges to a constant that represents somewhat of an average value. Note that the filter still reasonably well tracks both states p(t) and v(t); however, some of the behavior towards the end of the time series is not captured as the estimate is somewhat damped down (corresponding to the underestimated forcing).

To account for time-varying behavior in the parameter estimate, we can modify the augmented EnKF algorithm to include parameter tracking (see, e.g., [10]) by incorporating a random walk model for the parameter in the filter prediction step, such that

$$\theta_{j+1}^{(n)} = \theta_j^{(n)} + \xi_{j+1}^{(n)}, \quad \xi_{j+1}^{(n)} \sim \mathcal{N}(0, \sigma^2)$$
 (A.2)

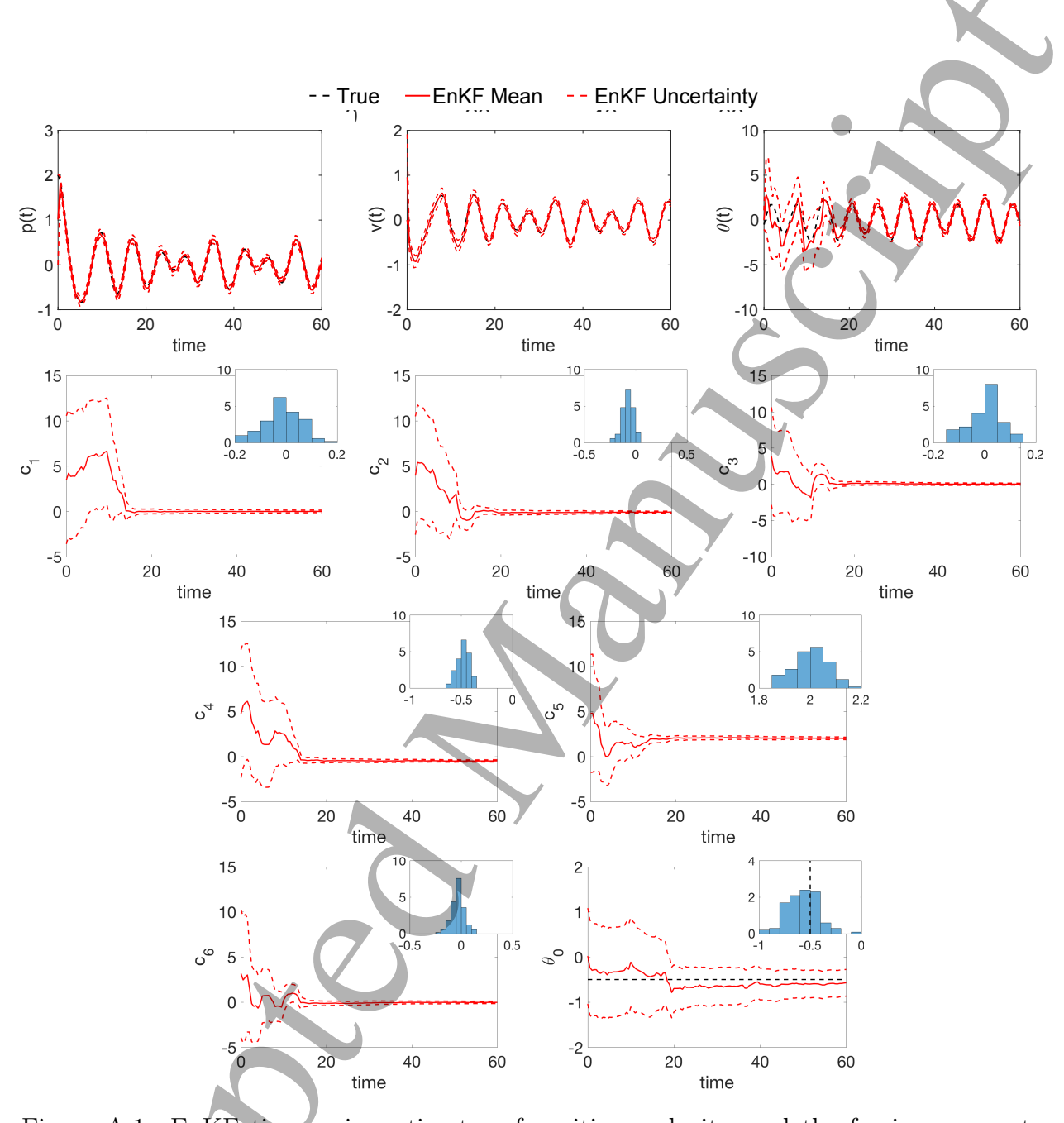


Figure A.1: EnKF time series estimates of position, velocity, and the forcing parameter $\theta(t)$, along with the six unknown coefficients in (14) and the initial condition θ_0 of the sinusoidal forcing parameter $\theta(t) = 2\sin(t) - 0.5\cos(2t/3)$ in (18) using the derivative-based augmentation approach when M = 3, given the data in Figure 3 and assuming a known period for $\theta(t)$. On each plot, the solid red line denotes the EnKF sample mean and the dashed red lines show ± 2 standard deviations around the mean. The plots for each coefficient, c_1, \ldots, c_6 , and for θ_0 also show the resulting histograms of the posterior samples at time t = 60.

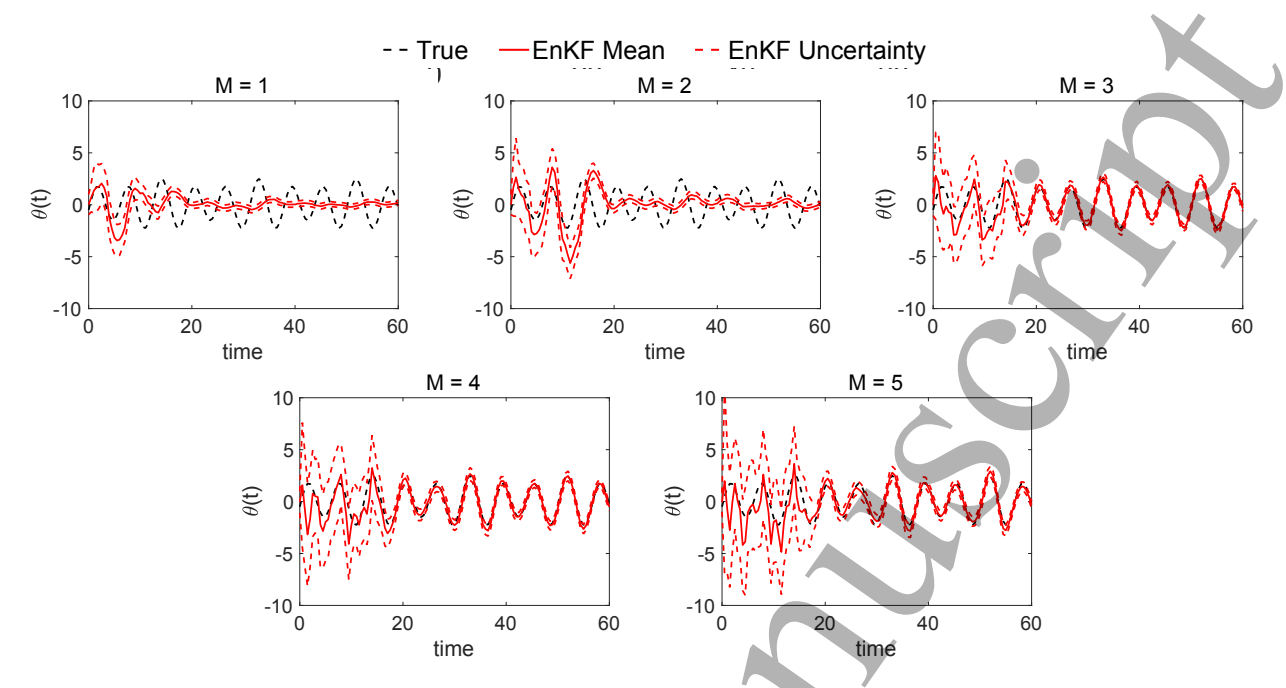


Figure A.2: EnKF time series estimates of the sinusoidal forcing parameter $\theta(t) = 2\sin(t) - 0.5\cos(2t/3)$ in (18) when using the derivative-based augmentation approach with different values of M, given the data in Figure 3 and assuming a known period for $\theta(t)$. On each plot, the solid red line denotes the EnKF sample mean, the dashed red lines show ± 2 standard deviations around the mean, and the dashed black line shows the true underlying $\theta(t)$.

for each ensemble member, n = 1, ..., N, where $\xi_{i+1}^{(n)}$ defines the parameter perturbation from time j to j+1. The success of parameter tracking with the EnKF relies significantly on the choice of the parameter noise model variance σ^2 [10], which must be manually selected before running the filter. Figure A.4 shows the resulting estimates of $\theta(t)$ when using parameter tracking with four different choices of σ (namely, when $\sigma = 0.1, 0.5, 1, \text{ and } 5$) and keeping all other filter settings (ensemble size, etc.) the same as in the previous numerical experiments. When $\sigma = 0.1$, we see that the underlying form and magnitude of $\theta(t)$ are not well captured. When $\sigma = 0.5$, the approximation improves but the form is still not well captured and the dynamics of the estimate lag behind the truth. For the larger values when $\sigma = 1$ and $\sigma = 5$, note that the overall dynamics of $\theta(t)$ are generally captured (with more error as σ increases) but the functional form is not well approximated in any case and the uncertainty bounds grow increasingly with σ . While some of these parameter estimates may be reasonable overall, note that this algorithm fails to well approximate the underlying functional form of $\theta(t)$. Further, since σ is fixed, we do not see a decrease in the EnKF uncertainty bounds over time. Comparing these results with those using the Fourier series-based approaches presented in this work (perhaps most visually comparable with the derivative-based augmentation results shown in Appendix A.1), we see that the Fourier series-based approximations have improved performance in capturing the functional form of the underlying TVP and by design give an approximation formula for $\theta(t)$ (or $d\theta/dt$) that can be used in making forward predictions with the system. We also see a decrease in uncertainty in the TVP approximation model coefficient estimates over time, as well as in the $\theta(t)$ approximations shown in Figure A.2 Table A.1: EnKF posterior sample means of the TVP model coefficients and initial value θ_0 for different values of M when using the derivative-based augmentation approach to estimate the sinusoidal forcing parameter $\theta(t) = 2\sin(t) - 0.5\cos(2t/3)$ in (18) given the data in Figure 3 and assuming a known period for $\theta(t)$. Numbers are rounded to four decimal places. Note that the Fourier series coefficients obtained using the formulas in (5) and (6) to approximate the known function for orders 3 and above correspond to $c_4 = -0.5$, $c_5 = 2$, and $c_k = 0$ for all other coefficients.

Coefficient	M = 1	M=2	M = 3	M = 4	M=5
c_1	0.1410	-0.0439	-0.0134	0.0590	-0.0324
c_2	-0.0073	0.1723	-0.0814	-0.0612	-0.0894
c_3	_	-0.0865	0.0034	-0.0505	0.0073
c_4	_	-0.1852	-0.4840	-0.4655	-0.5573
c_5	_	_	2.0026	2.0152	1.9659
c_6	_	_	-0.0318	0.0115	0.0038
c_7	_	_	_	0.1162	0.1577
c_8	_		(FN	0.1301	0.1571
c_9	_	F		_	-0.2124
c_{10}	_	-	7	_	0.1677
$ heta_0$	-0.0643	0.3544	-0.5720	-0.4168	-0.2902

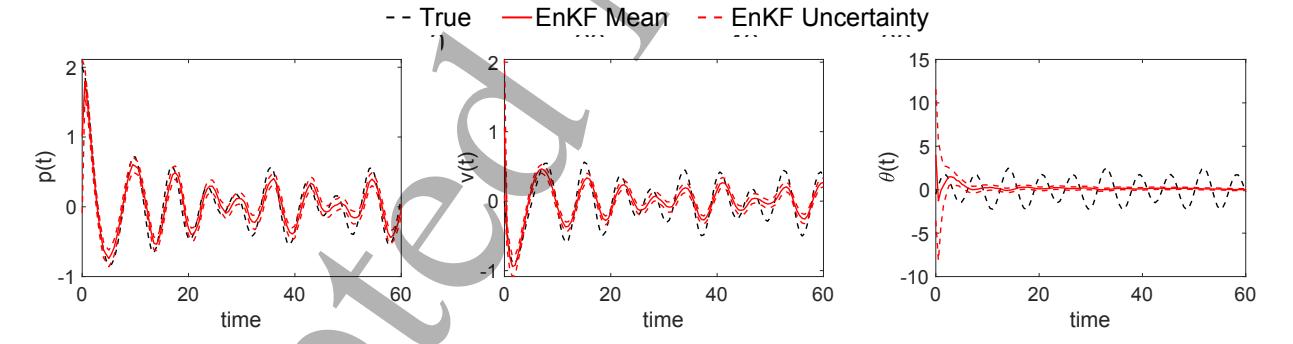


Figure A.3: EnKF time series estimates of position, velocity, and the forcing parameter $\theta(t)$ when estimating the sinusoidal forcing parameter $\theta(t) = 2\sin(t) - 0.5\cos(2t/3)$ in (18) using a standard augmented EnKF. On each plot, the solid red line denotes the EnKF sample mean and the dashed red lines show ± 2 standard deviations around the mean.

with the best fits resulting when M = 3, 4, and 5.

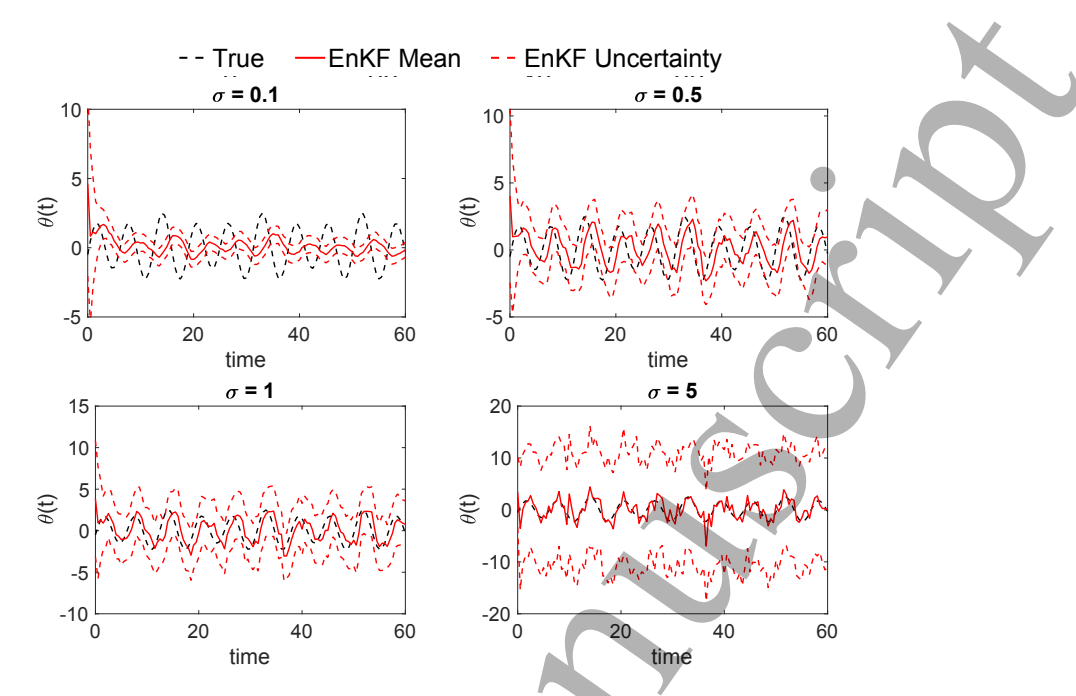


Figure A.4: EnKF time series estimates of position, velocity, and the forcing parameter $\theta(t)$ when estimating the sinusoidal forcing parameter $\theta(t) = 2\sin(t) - 0.5\cos(2t/3)$ in (18) using an augmented EnKF with parameter tracking. On each plot, the solid red line denotes the EnKF sample mean and the dashed red lines show ± 2 standard deviations around the mean.

A.3 Example Using Periodically-Forced Lorenz System with Chaotic Dynamics

As an additional test system, we consider a modified version of the Lorenz-63 equations [51], commonly studied in data assimilation as a simplified model for atmospheric convection that exhibits chaotic dynamics under certain parameterizations. In particular, we consider a periodically-forced Lorenz system of the type in [52] with governing equations given by

$$\frac{dx_1}{dt} = \sigma(x_2 - x_1) \tag{A.3}$$

$$\frac{dx_2}{dt} = \rho\theta(t)x_1 - x_1x_3 - x_2 \tag{A.4}$$

$$\frac{dx_3}{dt} = x_1 x_2 - \beta x_3 \tag{A.5}$$

where the constant parameters $\sigma = 10$, $\rho = 28$, and $\beta = 8/3$ are chosen so that the system exhibits chaotic behavior and $\theta(t)$ is a periodic forcing function. Assuming that σ , ρ , and β are known, our goal is to estimate $\theta(t)$ using the Fourier series-based TVP approximation technique. While in the previous examples the TVP of interest was additive with respect to the system states, note that here $\theta(t)$ is a multiplicative TVP. Further, here we assume that the system is partially observed, such that we are able to obtain observations of $x_2(t)$ and $x_3(t)$ (relating to the temperature variations) at some discrete times, but we cannot observe $x_1(t)$ (relating to convection) and thereby must track the behavior of $x_1(t)$ along with estimating the unknown TVP. Letting $\theta(t) = 1 + \varepsilon \cos(\omega t)$ (as studied in [52]) with

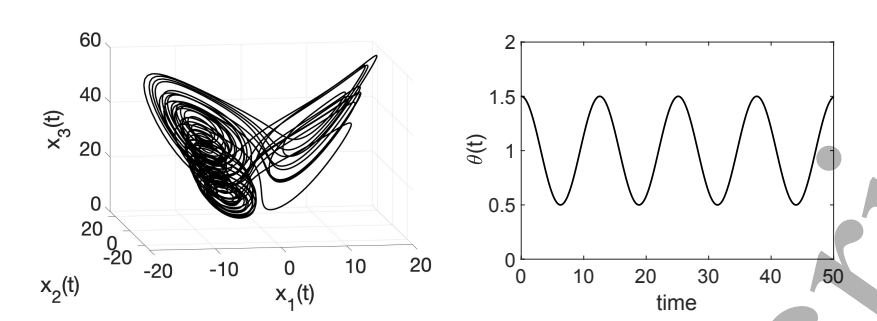


Figure A.5: Lorenz butterfly of the reference solutions for the forced Lorenz system in (A.3)–(A.5) with sinusoidal forcing parameter $\theta(t) = 1 + 0.5 \cos(0.5t)$.

 $\varepsilon = 0.5$ and $\omega = 0.5$ (corresponding to period $P = 4\pi \approx 12.57$), we simulate data from the forced Lorenz system in (A.3)–(A.5) by taking observations of the states x_2 and x_3 every 0.02 time units over the interval [0,50] (covering about 4 periods of $\theta(t)$) and corrupting with Gaussian noise (zero mean and variance taken to be 20% of the standard deviation of the true states, as before). Figure A.5 shows the Lorenz butterfly of the reference solutions (uncorrupted) and the forcing parameter $\theta(t)$.

Assuming a known period for $\theta(t)$, we apply the method in Section 3.1 using the formula in (10) to set $\omega_i = 0.5i$, i = 1, ..., M, and employ the TVP approximation model in (8) with increasing values of M, ranging from M = 1 (which involves three coefficients) through M = 5 (11 coefficients). Note that the Fourier series coefficients obtained when using the formulas in (5) and (6) to approximate the function $h(t) = 1 + 0.5\cos(0.5t)$, assuming that both h(t) and $P = 4\pi$ are known, gives a close approximation when Q = 1 with coefficients $c_0 = 1$, $c_1 = 0$, and $c_2 = 0.5$ (and using higher Q values yields similar approximations with $c_k = 0$ for the additional coefficients), so we expect comparable results using the Fourier series-based TVP approximation with a known period to estimate $\theta(t)$. We apply the EnKF similarly as before with an ensemble size of N = 100, with the aim of tracking the model states and estimating the unknown coefficients comprising the Fourier series-based model approximation of $\theta(t)$ for each value of M. Table A.2 lists the posterior sample mean of each coefficient for each M value, and Figure A.6 shows the resulting $\bar{\theta}_M(t)$ approximations in each case compared with the true $\theta(t)$.

As demonstrated in Table A.2, the filter well estimates the TVP approximation model coefficients, resulting in similar values to those expected from Fourier series expansion (with small approximation errors) for each M value. While not shown, the filter also well tracks all three model states (including the unobserved state x_1) for each M value. As shown in Figure A.6, while the lowest RMSE occurs when M=4 for this example, all of these M values result in reasonably close model approximations to the true $\theta(t)$ in this case. While we used an ensemble of size N=100 to compute the results as shown, we remark that similar results can be obtained using smaller ensembles (e.g., N=20 and above when M=1) but the performance degrades for too small an ensemble relative to the number of unknowns. Though these initial results are promising, in future work we will perform additional studies to verify the feasibility of the proposed technique for TVP estimation on larger-scale forced chaotic systems with more unknowns.

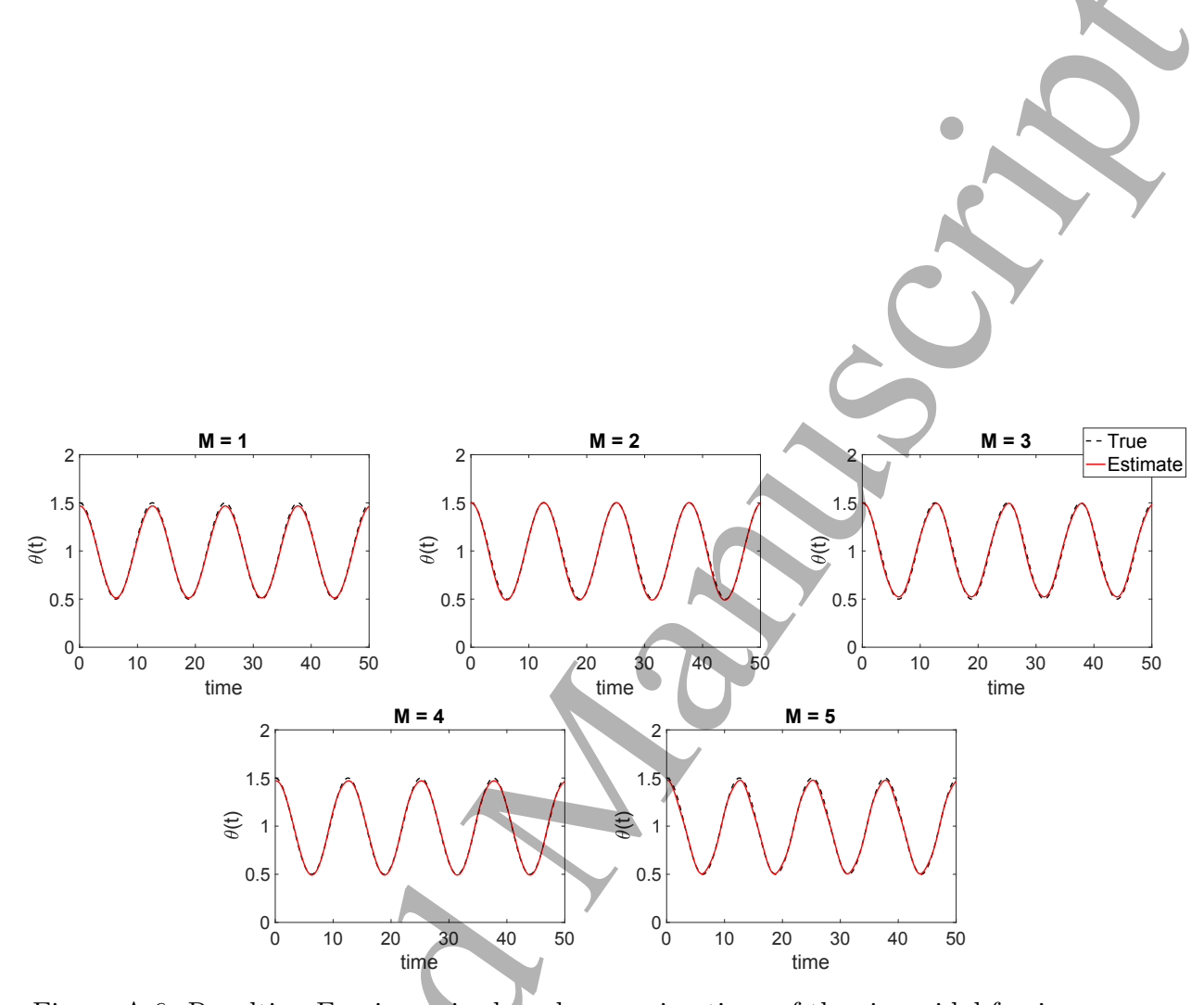


Figure A.6: Resulting Fourier series-based approximations of the sinusoidal forcing parameter $\theta(t) = 1 + 0.5\cos(0.5t)$ in (A.3)–(A.5) for different values of M assuming a known period for $\theta(t)$. On each plot, the solid red line denotes the TVP approximation $\bar{\theta}_M(t)$ computed using the posterior mean coefficient values in Table A.2 and the dashed black line shows the true underlying $\theta(t)$.



Table A.2: EnKF posterior sample means of the TVP model coefficients for different values of M when approximating the sinusoidal forcing parameter $\theta(t) = 1 + 0.5\cos(0.5t)$ in (A.3)–(A.5) assuming a known period for $\theta(t)$. Numbers are rounded to four decimal places. Note that the Fourier series coefficients obtained using the formulas in (5) and (6) to approximate the known function for orders 1 and above correspond to $c_0 = 1$, $c_1 = 0$, $c_2 = 0.5$, and $c_k = 0$ for all other coefficients.

Coefficient	M = 1	M=2	M=3	M=4	M = 5
c_0	0.9903	0.9930	1.0004	0.9971	0.9917
c_1	0.0060	-0.0173	-0.0177	-0.0001	-0.0076
c_2	0.4771	0.5056	0.4845	0.4913	0.4781
c_3		0.0076	0.0130	-0.0040	-0.0027
c_4	_	0.0041	0.0077	-0.0155	-0.0022
c_5	-	_	0.0143	0.0046	-0.0044
c_6		/ –	-0.0004	-0.0023	0.0035
c_7		_	_	0.0038	0.0128
c_8)-	_	_	-0.0002	0.0026
c_9	_	_	_	_	0.0017
c_{10}	_	_	_	_	0.0024
Scaled RMSE	0.0545	0.0452	0.0630	0.0392	0.0600

References

- [1] G. Sika and P. Velex. Instability analysis in oscillators with velocity-modulated time-varying stiffness-applications to gears submitted to engine speed fluctuations. *Journal of Sound and Vibration*, 318:166–175, 2008.
- [2] Y. Shen, S. Yang, and X. Liu. Nonlinear dynamics of a spur gear pair with time-varying stiffness and backlash based on incremental harmonic balance method. *International Journal of Mechanical Sciences*, 48:1256–1263, 2006.
- [3] J. Batouli, M. El Baz, and A. Maaouni. RLC circuit realization of a q-deformed harmonic oscillator with time dependent mass. *Physics Letters A*, 379:1619–1626, 2015.
- [4] J. Preiner, J. Tang, V. Pastushenko, and P. Hinterdorfer. Higher harmonic atomic force microscopy: Imaging of biological membranes in liquid. *Physical Review Letters*, 99:046102, 2007.
- [5] S. Altizer, A. Dobson, P. Hosseini, P. Hudson, M. Pascual, and P. Rohani. Seasonality and the dynamics of infectious diseases. *Ecology Letters*, 9(467-484), 2006.
- [6] Y. Zeng, X. Guo, Q. Deng, S. Luo, and H. Zhang. Forecasting of COVID-19: Spread with dynamic transmission rate. *Journal of Safety Science and Resilience*, 1(2):91–96, 2020.
- [7] D. Calvetti, A. P. Hoover, J. Rose, and E. Somersalo. Metapopulation network models for understanding, predicting, and managing the coronavirus disease COVID-19. *Frontiers in Physics*, 8:261, 2020.
- [8] D. Linaro, I. Biro, and M. Giugliano. Dynamical response properties of neocortical neurons to conductance-driven time-varying inputs. *European Journal of Neuroscience*, 47:17–32, 2018.
- [9] M. Shamir, O. Ghitza, S. Epstein, and N. Kopell. Representation of time-varying stimuli by a network exhibiting oscillations on a faster time scale. *PLOS Computational Biology*, 5(5):e1000370, 2009.
- [10] K. Campbell, L. Staugler, and A. Arnold. Estimating time-varying applied current in the Hodgkin-Huxley model. *Applied Sciences*, 10(2):550, 2020.
- [11] A. Arnold and L. Fichera. Identification of tissue optical properties during thermal laser-tissue interactions: an ensemble Kalman filter-based approach. *International Journal for Numerical Methods in Biomedical Engineering*, 38(4):e3574, 2022.
- [12] A. N. Bashkatov, E. A. Genina, V. I. Kochubey, and V. V. Tuchin. Quantification of tissue optical properties: perspectives for precise optical diagnostics, phototherapy and laser surgery. *Journal of Physics D: Applied Physics*, 49(50):501001, 2016.
- [13] S. Labiod, H. Boubertakh, and T. M. Guerra. Fourier series-based adaptive tracking control for robot manipulators. In *Proceedings of the 3rd International Conference on Systems and Control*, pages 968–972. IEEE, 2013.

- [14] A. Caruso, M. Bassetto, G. Mengali, and A. A. Quarta. Optimal solar sail trajectory approximation with finite Fourier series. *Advances in Space Research*, 67:2834–2843, 2021.
- [15] G. Konidaris, S. Osentoski, and P. Thomas. Value function approximation in reinforcement learning using the Fourier basis. In *Proceedings of the Twenty-Fifth AAAI Conference on Artificial Intelligence*, pages 380–385, 2011.
- [16] J. P. Boyd. *Chebyshev and Fourier Spectral Methods*. Dover Publications, Inc., Mineola, NY, second edition (revised) edition, 2001.
- [17] J. S. Hesthaven, S. Gottlieb, and D. Gottlieb. Spectral Methods for Time-Dependent Problems. Cambridge University Press, New York, 2007.
- [18] S. Liuzzo, R. Marino, and P. Tomei. Adaptive learning control of nonlinear systems by output error feedback. *IEEE Transactions on Automatic Control*, 52(7):1232–1248, 2007.
- [19] W. Chen, W. Li, and Q. Miao. Backstepping control for periodically time-varying systems using high-order neural network and Fourier series expansion. *ISA Transactions*, 49:283–292, 2010.
- [20] C.-L. Zhang and J.-M. Li. Hybrid function projective synchronization of chaotic systems with uncertain time-varying parameters via Fourier series expansion. *International Journal of Automation and Computing*, 9:388–394, 2012.
- [21] J. Chen and J. Li. Distributed consensus control of periodically time-varying multi-agent systems using neural networks and fourier series expansion. *Journal of the Franklin Institute*, 358:7170–7186, 2021.
- [22] G. Evensen. The ensemble Kalman filter for combined state and parameter estimation. *IEEE Control Systems Magazine*, 29:83–104, 2009.
- [23] M. A. Iglesias, K. J. H. Law, and A. M. Stuart. Ensemble Kalman methods for inverse problems. *Inverse Problems*, 29:045001, 2013.
- [24] C. Schillings and A. M. Stuart. Analysis of the ensemble Kalman filter for inverse problems. SIAM J Numer Anal, 55:1264–1290, 2017.
- [25] A. Abdulle, G. Garegnani, and A. Zanoni. Ensemble Kalman filter for multiscale inverse problems. *Multiscale Model Simul*, 18:1565–1594, 2020.
- [26] X.-L. Zhang, C. Michelen-Strofer, and H. Xiao. Regularized ensemble Kalman methods for inverse problems. *Journal of Computational Physics*, 416:109517, 2020.
- [27] A. Arnold, D. Calvetti, and E. Somersalo. Parameter estimation for stiff deterministic dynamical systems via ensemble Kalman filter. *Inverse Problems*, 30:105008, 2014.
- [28] A. Arnold and A. L. Lloyd. An approach to periodic, time-varying parameter estimation using nonlinear filtering. *Inverse Problems*, 34:105005, 2018.

- [29] A. Arnold. Using Monte Carlo particle methods to estimate and quantify uncertainty in periodic parameters. In *Advances in Mathematical Sciences*, pages 213–226. Springer, 2020.
- [30] M. Feng, P. Liu, S. Guo, L. Shi, C. Deng, and Ming B. Deriving adaptive operating rules of hydropower reservoirs using time-varying parameters generated by the EnKF. Water Resources Research, 53:6885–6907, 2017.
- [31] H. U. Voss, J. Timmer, and J. Kurths. Nonlinear dynamical system identification from uncertain and indirect measurements. *International Journal of Bifurcation and Chaos*, 14:1905–1933, 2004.
- [32] X. Bian, X. R. Li, H. Chen, D. Gan, and J. Qiu. Joint estimation of state and parameter with synchrophasors Part II: parameter tracking. *IEEE Transactions on Power Systems*, 26:1209–1220, 2011.
- [33] A. Arnold. Exploring the effects of uncertainty in parameter tracking estimates for the time-varying external voltage parameter in the FitzHugh-Nagumo model. In 6th International Conference on Computational and Mathematical Biomedical Engineering, pages 512–515, 2019.
- [34] D. Calvetti, A. Hoover, J. Rose, and E. Somersalo. Bayesian particle filter algorithm for learning epidemic dynamics. *Inverse Problems*, 37:115008, 2021.
- [35] A. Arnold. When artificial parameter evolution gets real: particle filtering for time-varying parameter estimation in deterministic dynamical systems. *Inverse Problems*, 39:014002, 2023.
- [36] A. Dourado and F. A. C. Viana. Physics-informed neural networks for missing physics estimation in cumulative damage models: A case study in corrosion fatigue. *J Comput Inf Sci Eng*, 20:061007, 2020.
- [37] G. A. Gottwald and S. Reich. Supervised learning from noisy observations: Combining machine-learning techniques with data assimilation. *Physica D*, 423:132911, 2021.
- [38] M. E. Levine and A. M. Stuart. A framework for machine learning of model error in dynamical systems. *Communications of the American Mathematical Society*, 2:283–344, 2022.
- [39] G. Evensen. Sequential data assimilation with a nonlinear quasi-geostrophic model using Monte Carlo methods to forecast error statistics. *Ocean Dynamics*, 99:10143– 10162, 1994.
- [40] G. Burgers, P. J. van Leeuwen, and G. Evensen. Analysis scheme in the ensemble Kalman filter. *Monthly Weather Review*, 126:1719–1724, 1998.
- [41] M. Katzfuss, J. R. Stroud, and C. K. Wikle. Understanding the ensemble Kalman filter. The American Statistician, 70:350–357, 2016.

- [42] L. F. Shampine. Vectorized adaptive quadrature in MATLAB. *Journal of Computational and Applied Mathematics*, 211:131–140, 2008.
- [43] R. K. Nagle, E. B. Saff, and A. D. Snider. Fundamentals of Differential Equations and Boundary Value Problems. Pearson, 6 edition, 2011.
- [44] W. E. Boyce and R. C. DiPrima. *Elementary Differential Equations and Boundary Value Problems*. John Wiley & Sons, New York, 7th edition, 2001.
- [45] P. Stoica and Y. Selen. Model-order selection: a review of information criterion rules. *IEEE Signal Processing Magazine*, 21(4):36–47, 2004.
- [46] J. Ding, V. Tarokh, and Y. Yang. Model selection techniques: An overview. *IEEE Signal Processing Magazine*, 35(6):16–34, 2018.
- [47] S. L. Brunton, J. L. Proctor, and J. N. Kutz. Discovering governing equations from data by sparse identification of nonlinear dynamics. *PNAS*, 113:3932–3937, 2016.
- [48] T. Schneider, A. M. Stuart, and J.-L. Wu. Ensemble Kalman inversion for sparse learning of dynamical systems from time-averaged data. *Journal of Computational Physics*, 470:111559, 2022.
- [49] N. Kantas, A. Doucet, S. S. Singh, J. Maciejowski, and N. Chopin. On particle methods for parameter estimation in state-space models. *Statistical Science*, 30(3):328–351, 2015.
- [50] D. Luengo, L. Martino, M. Bugallo, V. Elvira, and S. Sarkka. A survey of Monte Carlo methods for parameter estimation. EURASIP Journal on Advances in Signal Processing, 2020:25, 2020.
- [51] E. N. Lorenz. Deterministic nonperiodic flow. *Journal of the Atmospheric Sciences*, 20:130–141, 1963.
- [52] R. Saravanan, O. Narayan, K. Banerjee, and J. K. Bhattacharjee. Chaos in a periodically forced Lorenz system. *Physical Review A*, 31:520–522, 1985.